UNIVERSITY OF CALIFORNIA

Arterial Traffic Estimation Using Field Detector and Signal Phasing Data

A Research Report from the University of California Institute of Transportation Studies

Qijian Gan, Postdoc Researcher, PATH, University of California Berkeley

Alexander Skabardonis, Professor, Department of Civil and Environmental Engineering, University of California Berkeley

March 2019

PROJECT ID: UC-ITS-2018-01 | DOI: 10.7922/G2416V7N

ITS Berkeley Institute of Transportation Studies

Technical Report Documentation Page

1. Report No. UC-ITS-2018-01	**2. Government Accession No.** N/A	**3. Recipient's Catalog No.** N/A
4. Title and Subtitle Arterial Traffic Estimation Using Field Detector and Signal Phasing Data		**5. Report Date** February 2019
		6. Performing Organization Code ITS-Berkeley
7. Author(s) Qijian Gan, Ph.D. Alexander Skabardonis, Ph.D.		**8. Performing Organization Report No.** N/A
9. Performing Organization Name and Address Institute of Transportation Studies, Berkeley 109 McLaughlin Hall Berkeley, CA 94720		**10. Work Unit No.** N/A
		11. Contract or Grant No. UC-ITS-2018-01
12. Sponsoring Agency Name and Address The University of California Institute of Transportation Studies www.ucits.org		**13. Type of Report and Period Covered** Final Report
		14. Sponsoring Agency Code UC ITS

15. Supplementary Notes
DOI: 10.7922/G2416V7N

16. Abstract
In this project, a novel approach has been developed to estimate the traffic states on arterial road links controlled by signalized intersections using both loop detector data and signal phasing information. We derived a trapezoidal fundamental diagram that includes two occupancy thresholds to categorize the traffic states into three different regimes: uncongested, congested, and downstream queue spillback. The parameters used to compute these two thresholds are closely related to road geometry, detector layout, signal settings, and vehicle dynamics, which can be obtained from the field data. A case study was performed using field data from three intersections along Huntington Drive in the City of Arcadia in the I-210 Connected Corridors pilot. Flow-occupancy relations were obtained for both advance and stopline detectors at the intersection approaches, and it was found that advance detector information is more reliable because it is less impacted by the traffic signal. The proposed trapezoidal fundamental diagram was validated using a dataset with six months of detector data.

Arterials, traffic estimation, mathematical models		**18. Distribution Statement** No restrictions.	
19. Security Classif. (of this report) Unclassified	**20. Security Classif. (of this page)** Unclassified	**21. No. of Pages** 81	**22. Price** N/A

Form DOT F 1700.7 (8-72) Reproduction of completed page authorized

About the UC Institute of Transportation Studies

The University of California Institute of Transportation Studies (UC ITS) is a network of faculty, research and administrative staff, and students dedicated to advancing the state of the art in transportation engineering, planning, and policy for the people of California. Established by the Legislature in 1947, ITS has branches at UC Berkeley, UC Davis, UC Irvine, and UCLA.

Acknowledgements

This study was made possible through funding received by the University of California Institute of Transportation Studies from the State of California via the Public Transportation Account and the Road Repair and Accountability Act of 2017 (Senate Bill 1). The authors would like to thank the State of California for its support of university-based research, and especially for the funding received for this project. The authors would also like to thank Suzanne Petryk for performing some valuable simulations in AIMSUN, and Dr. Anthony Patire and Dr. Francois Dion for the model and data support.

Arterial Traffic Estimation Using Field Detector and Signal Phasing Data

UNIVERSITY OF CALIFORNIA INSTITUTE OF TRANSPORTATION STUDIES

March 2019

Qijian Gan, Postdoc Researcher, PATH, University of California, Berkeley

Alexander Skabardonis, Professor, Department of Civil and Environmental Engineering, University of California, Berkeley

[page intentionally left blank]

Table of Contents

LIST OF TABLES

LIST OF FIGURES

Executive Summary

In this project, a novel approach has been developed to estimate traffic states on arterial road links using both loop detector data and signal phasing information. The approach consists of the following two tasks: (i) estimate the traffic flow fundamental diagrams for arterial road links that are used to categorize traffic states into different regimes; (ii) develop estimation algorithms that utilize the proposed fundamental diagram and produce estimates of traffic states and vehicle queues for the traffic movements at a given intersection approach.

In the first task, the proposed fundamental diagram is trapezoidal, due to the presence of signal control. Two occupancy thresholds are proposed to categorize the traffic states into three different regimes: Uncongested, Congested, and Downstream Queue Spillback. The parameters used to compute these two thresholds are closely related to road geometry, detector layout, signal settings, and vehicle dynamics, which can be either measured or estimated from the field data. We point out that the proposed trapezoidal fundamental diagram is point-based, which can represent most of the traffic states on a link. However, when traffic is congested and the residual queue spills over the advance detectors, it fails to represent the traffic states on the link. Moreover, we carefully analyze the impacts of platoon dispersion, initial queue, and coordination level on the shape of the fundamental diagram. We analytically show that with minor platoon dispersion, our estimation of vehicle queueing time at advance detector is accurate. We also graphically show that the impact of initial queue can be ignored if we consider near-stationary traffic states. However, we find that poor coordination level can significantly degrade the traffic performance, which drifts the observed data points to the right with higher occupancies. As a case study, we select three intersections along Huntington Drive in the City of Arcadia in the I-210 Connected Corridors pilot. We carefully analyze the flow-occupancy relations at both advance and stopline detectors and decide to use the data from the former because it is less impacted by the traffic signal and the measurements are more reliable. In order to obtain the trapezoidal fundamental diagram, a key parameter to be estimated is the saturation flow rate. Therefore, we develop an algorithm that is used to estimate the saturation flow rates based on the data from advance detectors. Our results show that the estimated saturation flow rate varies a lot, ranging from 1200 veh/hr/ln to 2300 veh/hr/ln. According to the road geometry and the signal setting in the study site, we find that the low saturation flow rate may be caused by inappropriate detector placement, shared traffic movements, active pedestrian calls, and temporary lane blockages by the turning movements. To validate the estimation results, we first develop an algorithm to estimate the upper bounds of the flow-occupancy plots, which is considered to represent the actual fundamental diagrams. Then we calculate the Mean Absolute Percentage Error (MAPE) between the estimated trapezoidal fundamental diagram and the estimated upper bound. Our results show that generally the estimated trapezoidal fundamental diagram matches the estimated upper bound well. However, several exceptions are found which can be caused by insufficient data and poor coordination level.

In the second task, based on the proposed trapezoidal fundamental diagram, we further develop estimation algorithms for arterial road links. Especially, we use the two occupancy thresholds to categorize the traffic states at different types of detectors: three regimes for advance detectors, and two regimes for stopline detectors. We successfully validate these two thresholds by demonstrating a good fit to the data from the field and microsimulations for both advance and stopline detectors. Then with the consideration of different detector coverages and lane configurations, we develop algorithms that aggregate traffic states from individual detectors and produce estimates of traffic states and vehicle queues for the traffic movements at an intersection approach. Under the assumption of congested traffic and minor turning movements, we theoretically prove there exists a linear relation between the total vehicle queues and the travel times for multiple intersections with similar road geometries along an arterial corridor. We further select five intersections along Huntington Drive in Arcadia as the study site and successfully validate such a linear relation for the eastbound and west bound traffic using the field detector and Bluetooth travel time data. For traffic initialization, we develop an estimation and initialization framework for the microsimulation in AIMSUN. As an application example, we choose the I-210 AIMSUN network in the Connected Corridors project and generate simulated vehicles on the arterial road links in the City of Arcadia using the developed estimation and initialization algorithms.

Overall, the outcomes from this project provide valuable insights for both researchers and engineers to better understand arterial traffic. The proposed trapezoidal fundamental diagram reveals intrinsic characteristics of arterial traffic under signal control and has been thoroughly studies in this project. The developed estimation algorithms can work with the conventional data sources and is applicable under different detector layouts and lane configurations. The proposed estimation and initialization framework can be hooked up with large-scale simulation models since it fundamentally eliminates the step of simulation warmup and generates reliable and accuracy traffic states under good detector coverage and data quality. In addition, this study also provides building blocks for several future research directions, e.g., identification of lane blockage and queue spillback, optimal signal control based on the trapezoidal fundamental diagram, and a data fusion approach with probe trajectories to improve estimation accuracy.

1. Part I: Introduction

Traffic flow estimation is one of the key components in the Decision Support System (DSS) for Integrated Corridor Management (ICM). Accurate, robust, and timely estimates of traffic states are essential to allow traffic management agencies to make better decisions so as to reduce traffic congestion, road accidents and air pollution. Several methods have been proposed to estimate the traffic states on freeway segments. Fewer methods exist for arterials due to more complicated road geometries and the presence of signal control.

In practice, arterial traffic estimation is most needed when traffic incidents occur on freeways since it is important for traffic agencies to make sure the recommended response plans will not divert freeway traffic to the arterial road links that are already congested, which would worsen the traffic conditions. Furthermore, if traffic prediction is used in the DSS, it is important to make sure the simulated network starts with a good initial traffic state. The state-of-the-practice method in transportation simulation is to use a warm-up period with predefined demands and control settings. Such a method becomes inappropriate for real-time traffic management as the network size gets bigger due to the fact that it is more challenging to calibrate the network and takes a significantly longer time to reach a reasonable and stable traffic state. Therefore, it is critical to develop new methods to estimate arterial traffic states using existing road infrastructure and data sources.

Unlike freeway traffic, arterial traffic is impacted by many factors. First of all, traffic flow at an intersection approach is significantly impacted by signal control: a higher flow is expected if upstream demand is high and more green time is allocated. Besides that, various parties are involved at a given intersection: vehicles, cyclists, and pedestrians. Heavy cyclist and pedestrian traffic will significantly slow down the discharging process of certain traffic movements, e.g., right turns. As a result, a lower saturation flow is expected. Moreover, lower flows are expected when lane blockage and queue spillback occur. This is particularly true for left turn movements with insufficient green times. Therefore, estimating traffic states on arterial road links turns out to be more challenging than on freeways.

In this study, we want to tackle this problem by fusing signal phasing information from traffic signal controllers with data from loop detectors so as to provide accurate, robust, and timely estimates of traffic states. In the development of estimation algorithms, the following aspects are considered.

- First, the proposed algorithms should work under different detector layouts in the field. In field implementations, not all traffic movements have complete detector coverage. For example, left-turn movements are usually equipped with both stopline and advance detectors. But for through and right-turn movements, only advance detectors are available. This typical detector layout will also impact the signal control implemented in the field.

- Secondly, the proposed algorithms should work under different lane configurations of traffic movements. In the field, some lanes are dedicated for a certain traffic movement, while others are shared with multiple movements. As a results, traffic data from the corresponding detectors either represents an exclusive traffic movement, or the shared ones. This in turn will impact the development of our estimation algorithms since we need to aggregate traffic states from individual detectors to the approach level for each traffic movement.
- Thirdly, the proposed algorithm aims to work with conventional data from the controllers. In the literature, there have been studies that estimate vehicles queues at intersection approaches using detector data at a fine granularity, e.g., 30 seconds or even event based. However, these types of data are not easy to get since conventional controllers will aggregate and report the data at a longer interval, e.g., five minutes. Since the interval of five minutes consists at least two normal cycles at a signalized intersection, the estimated traffic states, e.g., vehicle queues, are in the "averaged" sense, not the actual ones at a particular time.
- Last but not least, the proposed algorithm should take into account the intrinsic characteristics of different types of detectors and try to maximize the information from them. For example, traffic at advance detectors is significantly different from that at stopline detectors, due to the fact that it is less impacted by the signal control. As a result, the flow-occupancy plots between these two types of detectors are very different. In our algorithm development, we will need to categorize the traffic states into different regimes for each detector type.

The trapezoidal fundamental diagram can be used to describe the traffic states on arterial road links. Two occupancy thresholds are proposed to divide the traffic states into three different regimes: Uncongested, Congested, and Queue Spillback. The required parameters are closely related to road geometry, detector layout, signal settings, and vehicle dynamics, which can be either measured or estimated from the field data. Note that the proposed trapezoidal fundamental diagram is point-based, which may fail to represent the actual vehicle queue on the link under certain circumstances. Furthermore, we will analyze potential impacts of platoon dispersion, initial queue, and coordination level on the shape of the trapezoidal fundamental diagram. In order to obtain the trapezoidal fundamental diagram, the saturation flow rate/ headway is the key parameter that should be calibrated/estimated from the field data. Therefore, we develop an algorithm that is used to estimate the saturation flow rates from individual detectors and select a study site along Huntington Dr in the city of Arcadia as an application example. Since data can be obtained from different types of detectors, e.g., advance and stopline detectors, we will perform a comprehensive analysis to show which data source is more reliable. Then we will show the estimation results of the detectors in the study site and point out potential causes of low saturation flow rates. For validation, we first propose an algorithm that estimates the upper bound of the flow-occupancy plot at a given detector, which is considered to represent the actual fundamental diagram. Then we calculate the MAPE between the estimated trapezoidal fundamental diagram and the upper bound. We will show that the estimated trapezoidal fundamental diagram generally matches the estimated upper

bound of the flow-occupancy plot well. However, we will also show some exceptions which may be caused by the lack of enough data points and poor coordination level.

Next, we move to the development of traffic estimation algorithms based on the above trapezoidal fundamental diagram. In particular, we apply the two occupancy thresholds to categorize the flow-occupancy plots into different regimes: three regimes for advance detectors, and two regimes for stopline detectors. Using data from the field and the AIMSUN microscopic simulation model, we first perform a fitness analysis to demonstrate how well the proposed two occupancy thresholds in categorizing the traffic states at advance and stopline detectors. Then with the consideration of different detector coverages and lane configurations, we develop our algorithm that aggregates the traffic states from individual detectors and produce traffic states and vehicle queues for different traffic movements at the approach level. With the assumption of congested traffic and no significant turning movements, we theoretically prove that there exists a linear relation between the total vehicle queues and the travel times for multiple intersections along an arterial corridor. Again, we select five intersections along Huntingtin Dr in Arcadia as a test site and demonstrate such a linear relationship for the eastbound and the westbound traffic. In addition, for traffic initialization in microsimulation, we propose an estimation-initialization framework in AIMSUN that generates simulated vehicles from the estimates of vehicle queues. As an application example, we demonstrate such a framework using the AIMSUN model in the I-210 Connected Corridors project and initialize the traffic states on the arterial road links in the city of Arcadia.

The rest of the report is organized as follows. In Part II, we focus on the estimation of the arterial traffic flow fundamental diagram. In Part III, we introduce the estimation algorithms for arterial traffic based on the proposed fundamental diagram. In Part IV, we draw our conclusions with some future research directions.

2. Part II: Estimation of Arterial Traffic Flow Fundamental Diagram

2.1 Problem Statement

In transportation networks, flow, speed, and density (or occupancy) are three common variables used to describe traffic states on a road link. Earlier in (Greenshields et al., 1935), it was found that a fundamental relation linking speed, flow, and density together exists in the field, which later is known as traffic flow fundamental diagram. Since then, a number of studies have confirmed its existence, particularly in freeway networks. Examples can be found in (Greenberg, 1959; Newell, 1961; Edie, 1961; Pipes, 1967; Payne, 1977; Castillo and Benitez, 1995; Lu et al., 2009; Dervisoglu et al., 2009; Li and Zhang, 2011; Yan et al., 2018). At the microscopic level, such a relation can be analytically derived from some prevailing car-following models, e.g., Pipes' model (Pipes, 1953), Optimal Velocity model (Bando et al., 1995), and Newell's model (Newell, 2002), under stationary traffic conditions (Cassidy, 1998). At the macroscopic level, numerous functions have been proposed to model the shape of

fundamental diagrams, either continuous (Greenshields et al., 1935; Greenberg, 1959; Newell, 1961; Pipes, 1967; Castillo and Benitez,1995) or discontinuous (Edie, 1961; Payne, 1977). To estimate key parameters of a fundamental diagram, i.e., free flow speed, critical density (or occupancy), jam density, and capacity, various types of data have been used, e.g., vehicle trajectory data (Lu et al., 2009) and loop detector data (Payne, 1977; Dervisoglu et al., 2009; Li and Zhang, 2011; Yan et al., 2018). To reduce noise impacts, some studies aggregated the data into different intervals, e.g., 10 seconds in (Lu et al., 2009) and 5 minutes in (Dervisoglu et al., 2009), while some others only used data points under near-stationary traffic conditions, e.g., (Payne, 1977; Li and Zhang, 2011; Yan et al., 2018). However, most of existing studies are for freeway road links, and few of them are for their arterial counterparts.

In arterial networks, vehicle movements are often interrupted by traffic signals. Because of that, the observed data points from a given detector, particularly for the one closer to the stopline, can scatter in a wide range in the flow-occupancy domain. Therefore, fundamental diagrams for freeway road links cannot directly be applied to the arterial ones. Using both loop detector and taxi data from Yokohama, Japan, Geroliminis and Daganzo (2008) showed that fundamental diagram of urban networks exists, which is known as the Macroscopic Fundamental Diagram (MFD). Since then, efforts have been devoted to various areas, e.g., analytical derivation of MFDs (Daganzo and Geroliminis, 2008; Helbing, 2009; Daganzo et al., 2011; Jin et al., 2013; Gan, 2014; Gan et al., 2017), empirical and numerical analysis of network inhomogeneity (Buisson and Ladier, 2009; Ji et al., 2010; Mazloumian et al., 2010; Gayah and Daganzo, 2011b,a; Geroliminis and Sun, 2011; Knoop et al., 2012) on the shape of MFDs, and etc. However, the aforementioned studies are for urban networks, not for individual arterial road links.

In the field, numerous detectors have been installed at intersection approaches to facilitate the control of conflicting traffic movements. For example, advance detectors are normally installed about 200 feet upstream from the stopline to detect vehicle arrivals, while stopline detectors are installed to detect vehicle's presence. Depending on the configuration, these detectors can consist of different loops: normally signal loop for advance detectors, and multiple loops for stopline detectors. As a result, they have different lengths, which will impact their detection accuracy. In the literature, few efforts have been devoted to analytically deriving or empirically illustrating the shape of fundamental diagrams for arterial road links. As shown in Wu et al. (2011), the major reason is because the wide scattering data points in the flow-occupancy plots make it difficult to justify the shape of fundamental diagrams. By eliminating the queue-over-detector (QOD) impact inside the cycle-based data from loop detectors, results in (Wu et al., 2011) have demonstrated that fundamental diagrams for arterial road links should exist. However, the regime with heavy congestion was not detected, and no analytical models were provided.

In this part, we aim to fill this gap. We want to provide a general approach to derive the fundamental diagrams (i.e., the flow-occupancy relation) for arterial road links. At a given intersection approach, we assume vehicles arrive in platoons with no dispersion, which is

particularly true when signals are coordinated and intersections are narrowly-spaced. Based on this assumption, we derive a trapezoidal fundamental diagram, the break points of which are determined by a set of parameters including saturation flow rate, saturation speed, green ratio, detector length, and average vehicle length. Furthermore, we discuss potential impacts of platoon dispersion, initial queue, and coordination level on the shape of the fundamental diagram. We demonstrate that our estimation of vehicle queuing time at advance detectors is accurate with minor platoon dispersion, and the impact of initial queues can be ignored if we consider near-stationary traffic conditions. However, poor coordination level does degrade the traffic performance, which shifts the observed data points to the right with higher occupancies. Three intersections along Huntington Dr in the City of Arcadia are chosen as the study site, which is within the I-210 Connected Corridors Pilot[1]. The data has been collected for one year and a half from Arcadia's TCS Server and is divided into two subsets: data in the first twelve months is used for calibration, while the rest is used for validation. Before calibration and validation, we first analyze the flow and occupancy relations at both advance and stopline detectors, with the consideration of potential impacts from traffic congestion, detector length, and distance to the stopline. We find that measurements from advance detectors are more reliable, and the relation between flow and occupancy is much clearer. In order to obtain the trapezoidal fundamental diagram, a key parameter to be estimated is the saturation flow rate. Therefore, we select observations from the calibration dataset with occupancies in the congested region to estimate the corresponding saturation flow rates for different advance detectors and signal control plans. Our results show that the saturation flow rate varies a lot among intersections as well as signal control plans. For validation, we first estimate the upper bounds of flow-occupancy plots in the validation dataset, which are considered to represent the actual fundamental diagrams. Then we calculate the corresponding MAPE with the estimated trapezoidal fundamental diagrams. Our results demonstrate that the estimated trapezoidal fundamental diagram generally matches the field data well.

2.2 Derivation of Arterial Traffic Flow Fundamental Diagram

In this section, we introduce a general framework to derive traffic flow fundamental diagrams for arterial road links. In particular, we focus on the flow-occupancy relationship since they are the two direct and conventional measurements from loop detectors in the field.

Figure 1 illustrates the proposed trapezoidal fundamental diagram for arterial road links. From the figure, we can find that the original fundamental diagram is triangular, with a maximum flow rate of q_s. Due to the presence of signal control, the actual capacity is reduced to q_c, and as a result, the fundamental diagram becomes trapezoidal. In the literature, such a trapezoidal fundamental diagram has been used to match the field data in Figure 11 in (Wu et al., 2011). However, in order to determine its shape, we need to estimate three of the following four

[1] Connected Corridors. https://connected-corridors.berkeley.edu/. *Last visited on 2018/09/17*.

parameters: $\{q_s, q_c, Occ_1, Occ_2\}$. In the following, we will provide the details on how to determine these parameters.

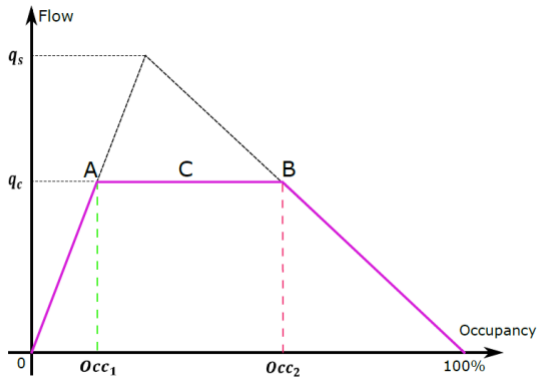

Figure 1 Proposed trapezoidal traffic flow fundamental diagram for arterial road links.

2.2.1 Determination of Saturation Flow Rate

In the Highway Capacity Manual (HCM) (TRB, 2000), the saturation flow rate q_s is determined as:

$$q_s = \frac{3600}{h_s} \quad \text{(vphg)} \qquad (1)$$

Where h_s is the saturation headway, that is the minimum headway that vehicles discharge assuming a queue of vehicles and the signal is green. A number of studies have shown that the saturation headway is location dependent and may vary from 1.8 to 2.4 seconds (Al-Ghamdi, 1999; TRB, 2000; Tong and Hung, 2002; Lin and Thomas, 2005; Jin et al., 2009). Also, the saturation flow rate (or headway) is lane specific since vehicle's discharging pattern on a specific lane is closely related to its configuration of traffic movements.

2.2.2 Determination of Link Capacity

The effective green time is the actual green time minus the start-up delay plus the utilization of the yellow. Start-up lost time is the time from when traffic signal turns green and vehicles discharge at their minimum headway. Utilization of the yellow is the time that vehicles continue to cross the intersection after the onset of the yellow interval. We assume that the start lost time and utilization of the yellow time are equal resulting in the effective green time being equal to the actual green time. The link capacity is equal to the discharge flow (saturation flow) during the green time:

$$q_c = q_s * \frac{G}{C}, \quad \text{(vph)} \qquad (2)$$

where G is the green time, and C is the cycle length.

2.2.3 Determination of Critical Occupancies

When the flow rate reaches capacity, it can span over a wide range of occupancies, from Point A to Point B in Figure 1. Specifically, the two critical occupancies at points A and B correspond to two significantly different platoon arrival patterns. As a first step, we have the following assumptions:

(i) No initial queue at the beginning of red time.

(ii) Platoon arrivals from upstream intersections with no dispersion.

2.2.3.1 Ideal case: Platoon Arrival with Perfect Coordination

As shown in Figure 2(a), the first case is an ideal case when we have perfect coordination along an arterial corridor with the maximum green wave. Under such a condition, vehicle platoons from the upstream can cross the intersection freely without stopping, and no queue is formed. If we assume the total lost time within a phase is close to the yellow and all red time, the effective green time for vehicle passage is G (sec). Furthermore, the saturation speed is denoted as v_s (mph), the average vehicle length is denoted as L (feet), and the detector length is denoted as D (feet). Since the effective green time is fully used, the total time T_{pass} for vehicles passing the advance detector freely within one cycle is

$$T_{pass} = \frac{(L+D)*3600}{v_s*5280} * \frac{q_s*G}{3600} = \frac{(L+D)Gq_s}{5280v_s}. \quad (3)$$

Therefore, the corresponding occupancy (i.e., Point A in Figure 1) is computed as

$$Occ_1 = \frac{T_{pass}}{C} = \frac{(L+D)q_sG}{5280v_sC}. \quad (4)$$

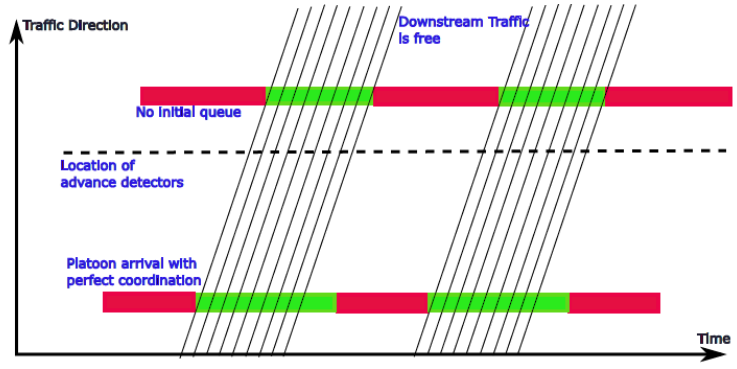

a. Ideal case

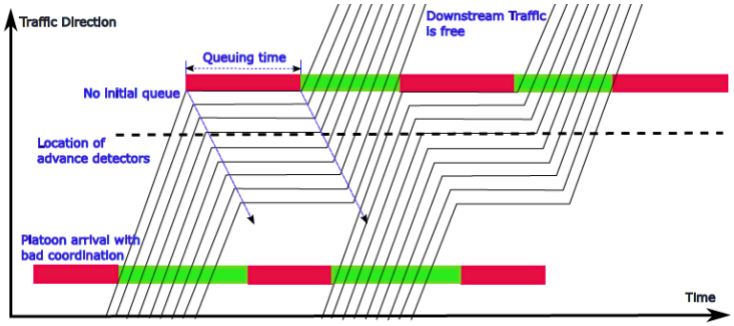

b. Worst case

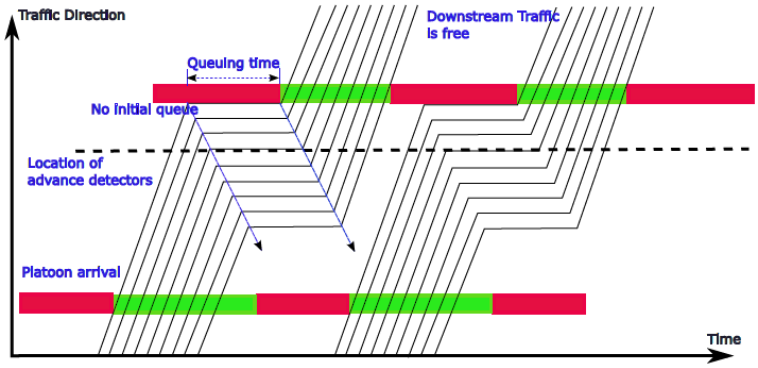

c. Normal case

Figure 2 Platoon arrival patterns under different levels of coordination.

2.2.3.2 Worst Case: Platoon Arrival with the Longest Waiting Time

As shown in Figure 2(b), the second case is the signal coordination is so poor that the vehicle platoon hits the starting time of the red interval every time it arrives at the intersection. As a result, a queue forms and propagates back to advance detectors. In such a case, the time when an advance detector is occupied can be separated into two different portions: (i) queuing time, i.e., it is $C - G$ in this case; and (ii) passage time, i.e., T_{pass} in Equation 3. Therefore, the corresponding occupancy (Point B in Figure 1) is computed as

$$Occ_2 = \frac{T_{pass}+C-G}{C} = 1 - \frac{G}{C} + \frac{(L+D)q_s G}{5280 v_s C}. \quad (5)$$

Please note that since we consider no platoon dispersion, the shock-wave speed (when a moving vehicle joins the tail of a queue) is the same as the rarefaction wave speed (when a queued vehicle is released at the saturation flow rate). Therefore, we will see two parallel arrows in Figure 2 and some of the following figures.

2.2.3.3 Normal Case: Platoon Arrival Waiting for a Certain Proportion of Red Time

As shown in Figure 2(c), a more general case is that the vehicle platoon randomly hits the red interval, and therefore, has to wait for a portion of red time. Depending on when the vehicle platoon hits the red interval, the queuing time varies and can be computed as

$$T_{waiting} = \alpha(C - G), \quad (6)$$

where α is the portion of red time the vehicle platoon has to wait and is in the range of $(0,1)$. Then, the corresponding occupancy (Point C in Figure 1) is computed as

$$Occ = \frac{T_{pass}+T_{waiting}}{C} = \alpha(1 - \frac{G}{C}) + \frac{(L+D)q_s G}{5280 v_s C}. \quad (7)$$

2.2.4 Formulation

After we determine the capacity and the two critical occupancies, the trapezoidal traffic flow fundamental diagram can be formulated as below:

$$q\left(Occ, \frac{G}{C}\right) = \begin{cases} q_c \frac{Occ}{Occ_1}, & Occ \in [0, Occ_1] \\ q_c, & Occ \in (Occ_1, Occ_2] \\ q_c \frac{1-Occ}{1-Occ_2}, & Occ \in (Occ_2, 1] \end{cases}. \quad (8)$$

From Equation 8, the outflow rate is impacted by the green ratio, i.e., $\frac{G}{C}$, which plays an important role in determining the capacity flow and the two critical occupancies. It is also clear to see that when the green ratio converges to 1, the fundamental diagram in Equation 8 becomes the traditional triangular one.

Using these two critical occupancies, the flow-occupancy relation can be categorized into three different regimes:

(i) Uncongested regime with $Occ \leq Occ_1$.

In this regime, vehicles can travel across advance detectors freely. There may be a minor queue at the stopline during the red time period. But the allocated green time is able to clear the queue since vehicle's arrival rate is relatively low.

(ii) Congested regime with $Occ_1 < Occ \leq Occ_2$.

In this regime, traffic is congested at the given approach, with a queue that will spread to the advance detectors for a certain period of time. Several reasons will lead to this situation. For example, there may be a persisting short queue that cannot be cleared by the green time in each cycle. Also, bad signal coordination will force the upstream vehicle platoon to stop every time they reach the intersection. If the upstream arrival rate is high, it is easy to generate a queue that will occupy the advance detectors for a certain time. However, we need to be sure that in this regime the downstream road link is uncongested, and thus vehicles at the stopline can exit freely when the signal turns green.

(iii) Downstream spillback regime with $Occ_2 < Occ \leq 1$.

In this regime, the occupancies are very high, but the corresponding flows are relatively low. Such a case is caused by downstream queue spillback to the targeted intersection. As a result, the outflow is restricted by the downstream traffic, depending on whether there is enough space to accommodate the exiting vehicles. Meanwhile, there should be a long queue at the given approach that spreads to the advance detectors and occupy it for a long time.

2.2.5 Limitation in Point Detection

The trapezoidal fundamental diagram in Figure 1 is point-based, which means it is derived from measurements at fixed detectors. For most of the cases, the point-based state can represent the correct state on a link. However, it fails when the allocated green time cannot clear all vehicles in a cycle and the residual queue is so long that it spills over the advanced detectors. In this case, at the advance detectors, no matter how long the residual queue is, the detected

occupancy and flow rate remain to be Occ_2 and q_c respectively, i.e., point B in Figure 1. In other words, point B in Figure 1 represents a wide range of heavy traffic states on a link.

However, this limitation is not that critical to the applications/methods developed based on the proposed trapezoidal fundamental diagram. Take optimal signal control as an example. When the optimized green time is long enough to clear the arrival flow, the residual queue shrinks gradually cycle by cycle. Finally, the traffic will stabilize itself on the left-hand side of point B, which demonstrates the improvement by the optimal signal setting.

2.3 Discussion of Potential Impacts

In this section, we analyze key factors that will impact the derived fundamental diagram. Particularly, we are interested in the following factors: platoon dispersion, initial queue, and coordination level.

2.3.1 Impact of Platoon Dispersion

Considering the case of closely spaced intersections, we assume vehicles arrive at an intersection approach in platoon with no dispersion. But actually, platoon dispersion with a larger vehicle gap will occur as vehicles escape from the upstream intersection. Under such a case, we consider the arrival speed is still the same, but the arrival flow rate is smaller due to the enlarged vehicle gaps. In Figure 3, we graphically illustrate of the impact of platoon dispersion on the estimation of queue waiting time in Equation 6. As shown in Figure 3(a), since the vehicle gap is larger, the actual queuing time is smaller than the proposed one. Let's denote the distance between the stopline and the advance detectors as d, the rarefaction wave speed at the saturation flow as w_1, and the shock wave speed at the arrival flow as w_2. The values of w_1 and w_2 are illustrated in Figure 3(b). Then the time difference between the actual queuing time and the proposed one used in Equation 6 can be calculated as

$$T_{diff} = \frac{d}{w_2} - \frac{d}{w_1} = \frac{d(w_1 - w_2)}{w_1 w_2}$$

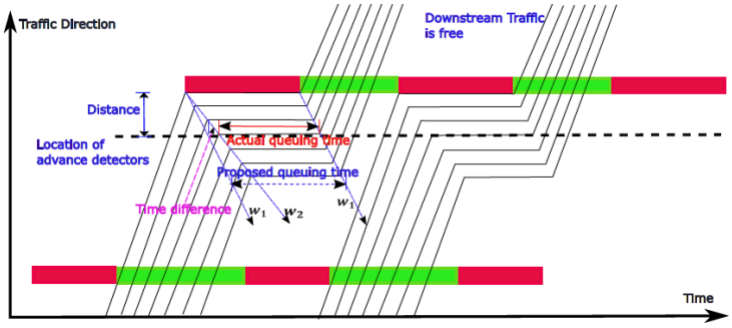

a. Time difference in the space-time diagram

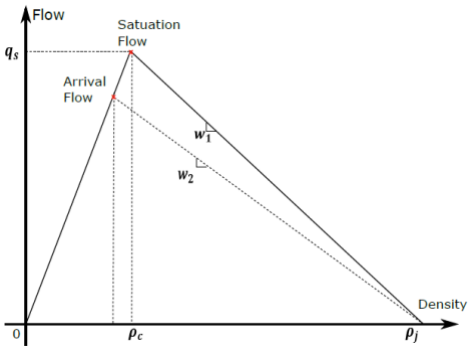

b. Two different wave speeds

Figure 3 Illustration of platoon dispersion

From Equation 9, we can see that the time difference is closely related to the shock wave speed w_2. The lower w_2, the lager T_{diff}. In other words, if the platoon dispersion is significant with a lower arrival rate, which leads to a lower w_2, the error in estimating the queuing time from the advance detectors will increase.

Assume the saturation flow rate q_s=1800veh/hr/ln, jam density ρ_j = 180veh/mile, critical density ρ_c = 60veh/mile, wave speed w_1= 15mph, and d = 200feet. If the wave speed w_2=12mph, which corresponds to an arrival rate of 1543veh/hr/ln, the time difference T_{diff}= 2.27sec. The relative error is very small, only 2.5% if the cycle length is C = 90sec. It is even smaller if the cycle length is longer. But if we set w_2= 6mph, which corresponds to an arrival rate of 900veh/hr/ln, the time difference T_{diff}= 13.6sec and the relative error is 15%. Therefore, significant platoon dispersion will degrade the estimation accuracy of queuing time at advance detectors (Equation 6), which will lead to unrealistic estimates of the two critical occupancies in Figure 1.

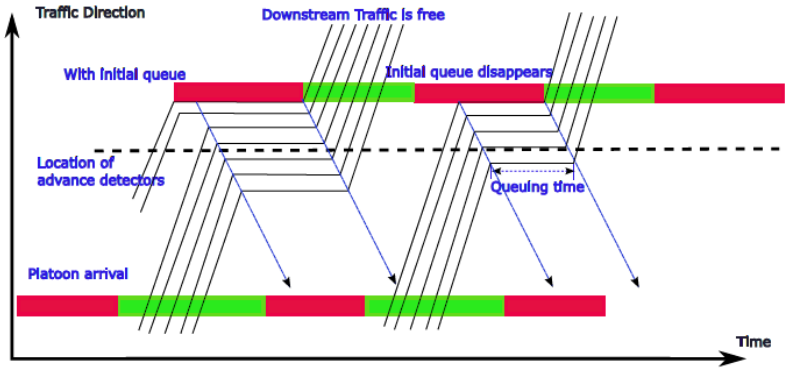

a. Demand lower than capacity

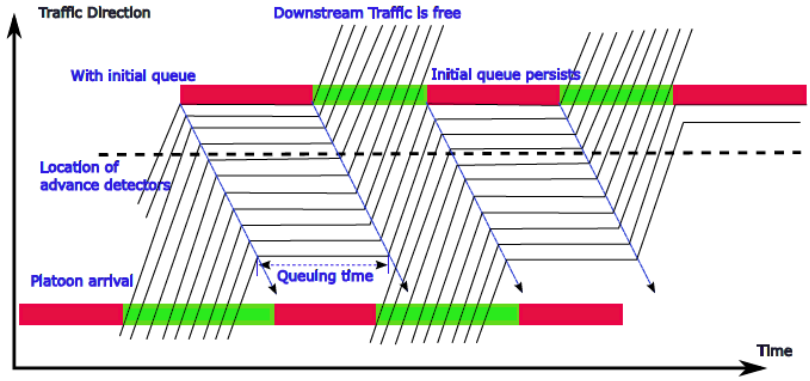

b. Demand at capacity

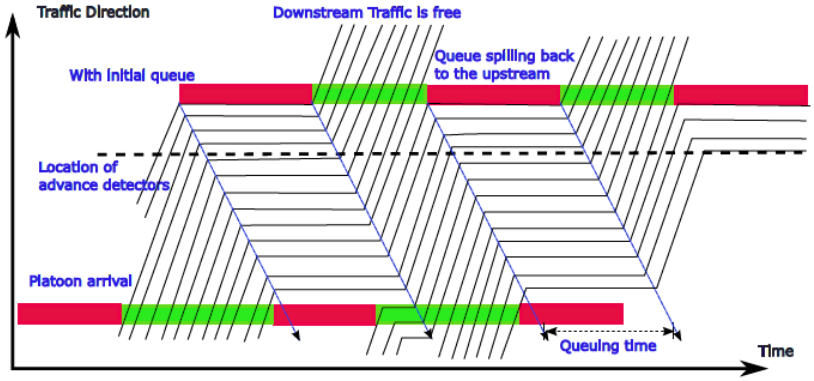

c. Demand greater than capacity

Figure 4 Platoon arrival patterns under the existence of initial queues.

2.3.2 Impact of Initial Queues

In Figure 4, we provide platoon arrival patterns under the existence of initial queues. As shown in Figure 4(a), when the upstream demand (i.e., arrival rate) is lower than the intersection capacity, the initial queue will finally disappear because the green time at the targeted intersection is long enough to dissipate these queued vehicles. Therefore, the impact of initial queue can be eliminated as time elapses.

However, when the upstream demand reaches the intersection capacity, as shown in Figure 4(b), the initial queue persists over time. As a result, the queuing time at the advance detectors reaches its maximum, which is the whole red time period. In this case, the corresponding flow and occupancy is Point B in Figure 1.

In an extreme case when the demand is greater than the intersection capacity, as shown in Figure 4(c), the queue grows as time elapses and finally partially blocks the upstream intersection. No matter whether an initial queue exists or not, the queuing time at the advance

detectors will be the total red time period. Thus, the corresponding flow and occupancy will be Point B at Figure 1.

As discussed above, upstream demand dominates the traffic dynamics in the downstream intersection approach. If we consider stationary traffic states, the impact of initial queue can be ignored.

2.3.3 Impact of Coordination Level

In Figure 5, we provide the arrival patterns of small platoons under different coordination levels. The first is an ideal case with perfect signal coordination, under which vehicle platoons can cross the intersections without stopping. The corresponding arrival pattern is provided in Figure 5(a). In this case, since the arrival rate is less than the capacity, the corresponding flow and occupancy is point D in Figure 5(b).

The second case is under normal situations that vehicle platoons hit the red time occasionally and have to wait for a short time period, which is shown in Figure 5(c). Since the arrival flow rate is smaller than the capacity, the outflow rate is the same as the first case. However, the corresponding occupancy is higher due to the waiting time. Therefore, it corresponds to Point E in Figure 5(d).

The third case is the worst with bad coordination. As shown in Figure 5(e), vehicle platoons arrive at the intersection approach right at the beginning of the red interval. As a result, the platoon has to wait for the whole red time. Since the arrival flow rate is smaller than the capacity, the next green time can clear the residual queue. However, the corresponding occupancy is the highest. This case corresponds to Point F in Figure 5(f).

The above patterns can be found from the field data. For example, in Figure 8(a), there are many points under the traffic flow fundamental diagram (i.e., the upper bound of the flow-occupancy plot). Note that as illustrated in Figure 5(a,c,e), in order to see these traffic patterns from advance detectors, the arrival flow rate should be high enough so that the vehicle queue can spill back to the advance detectors. That also explains why we cannot see a wide range of occupancy for low arrival flow rates in Figure 8(a).

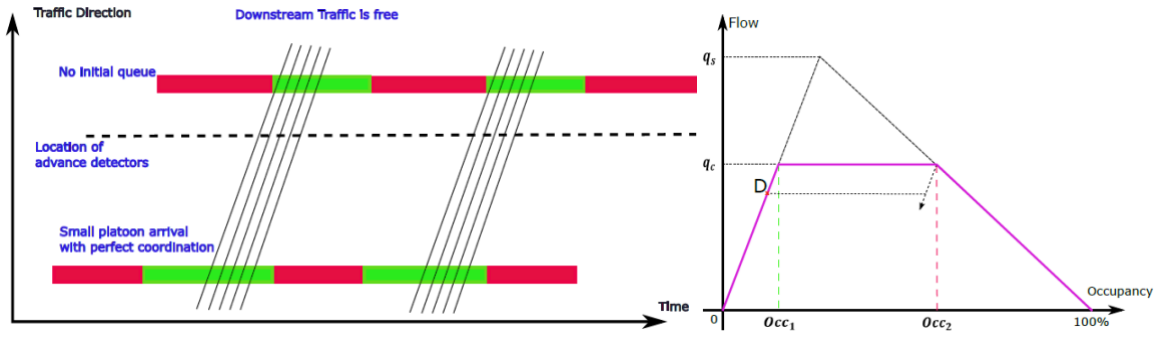

(a) Without stopping: Space-Time Diagram (b) Without stopping: Fundamental Diagram

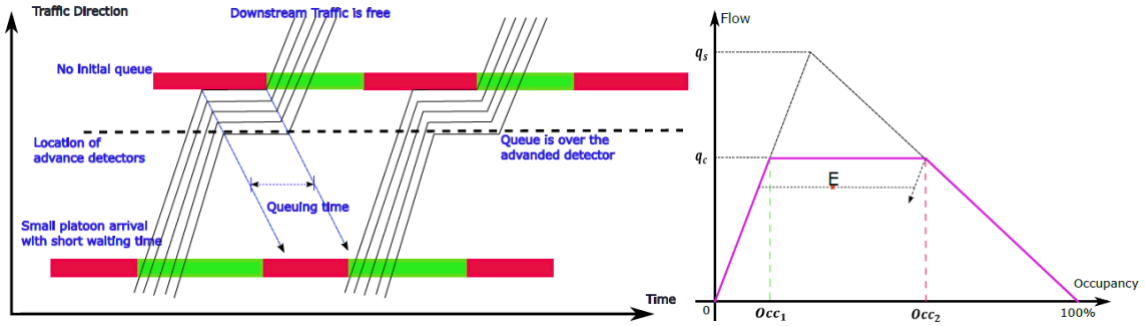

(c) With a short waiting time: Space-Time Diagram (d) With a short waiting time: Fundamental Diagram

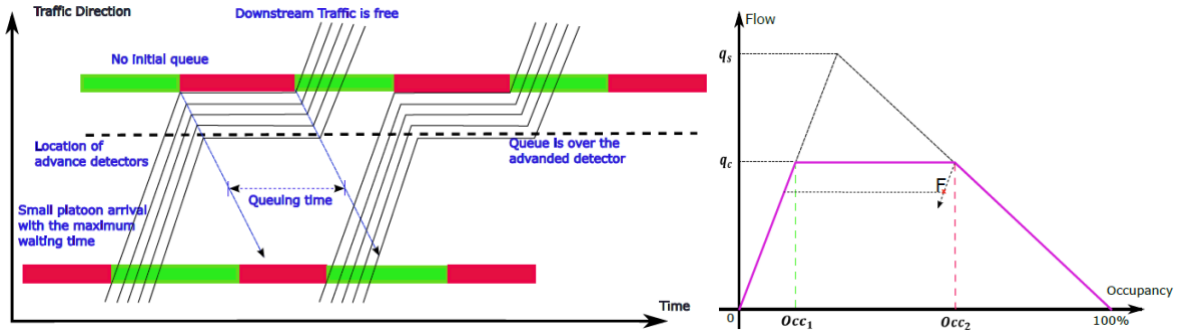

(e) With the longest waiting time: Space-Time Diagram (f) With the longest waiting time: Fundamental Diagram

Figure 5 Arrival patterns of small platoons under different coordination levels.

2.4 Study Site

This section introduces the study site that will be used to calibrate and validate the proposed trapezoidal fundamental diagram in Section 2.2. It consists of three parts: (a) road geometry and detector layout, (b) signal phase settings, and (c) data source.

2.4.1 Road Geometry and Detector Layout

In Figure 6, we provide the road geometry of three intersections along Huntington Dr in the City of Arcadia, CA: Huntington Dr&Santa Anita Ave, Huntington Dr&First Ave, Huntington Dr&Second Ave. Meanwhile, detector locations are mapped into the figure. From the figure, we find that most of the intersection approaches contain only advance detectors and stopline detectors for exclusive left-turn movements. Very few of them, e.g., the eastbound and westbound approaches at Huntington Dr&Second Ave, are covered by stopline detectors that are used to detect through and/or right-turn movements. Detailed configuration, including detector type, detected movements, distance to stopline, number of lanes, and detector length, is provided in Table 1

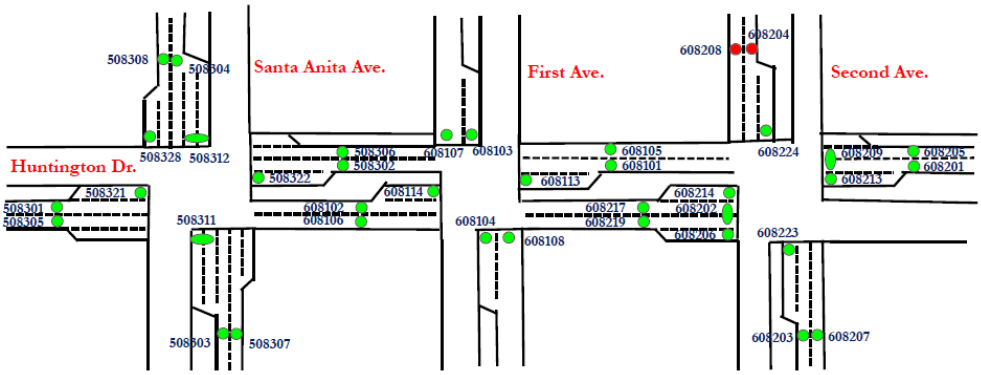

Figure 6 Road geometry and detector layout at three intersections along Huntington Dr in Arcadia.

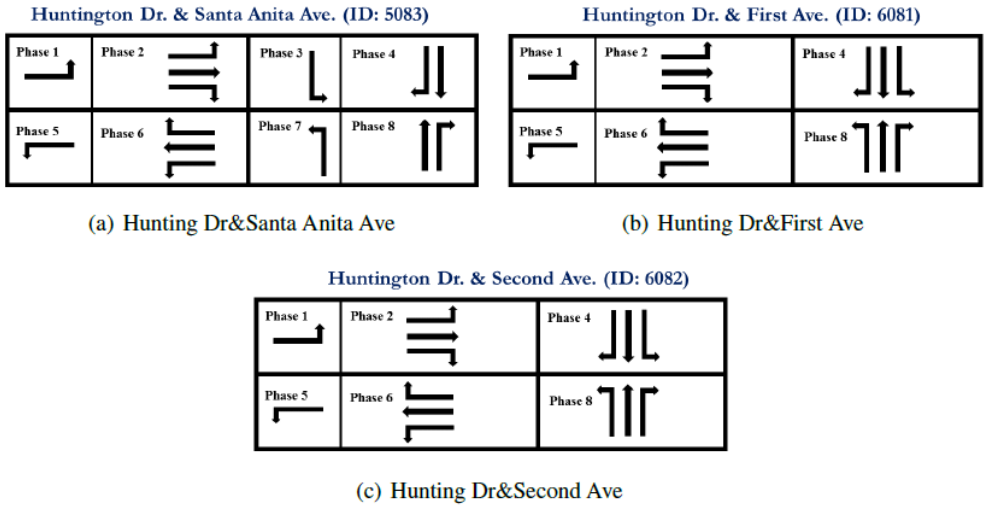

Figure 7 Signal phase settings at the three intersections in Arcadia.

2.4.2 Signal Phase Settings

Through the I-210 Connected Corridors project, we are able to collect signal timing sheets and intersection detection layouts from LA County, Pasadena, Arcadia, and other jurisdictions. Figure 7 illustrates signal phase settings of the three intersections. From the figure, we can find that there are eight phases for the intersection between Huntington Dr and Santa Anita Ave, while there are only six phases for the other two intersections. In the eastbound and westbound directions, the left-turn movements at the three intersections are designed as "Protected-Permitted", which means left-turn vehicles still can cross the intersection if there are enough gaps in the opposite traffic. In the northbound and southbound directions, the left-turn movements at the intersection between Huntington Dr and Santa Anita Ave are "protected" only, while the corresponding ones at the other two intersections are "permitted". Detailed signal phase plans at these intersections are provided in Table 2. From the table, we can see that there are four different signal plans, which are used for six different time periods in a daily sequence of $E \rightarrow P_2 \rightarrow P_1 \rightarrow P_3 \rightarrow P_1 \rightarrow E$. The allocated green times are different among the timing plans.

All timing plans except “E” at the three intersections are designed for coordinated control with a common cycle length.

Table 1 Detector configurations at the three intersections.

Huntington Dr&Santa Anita Ave (ID: 5083)						
Traffic Direction	Detector ID	Detector Type	Detected Movements	Distance To Stopbar(ft)	Number Of Lanes	Detector Length(ft)
Eastbound	508301	Advance	LT,TH,RT	185	1	7
	508305	Advance	LT,TH,RT	185	1	7
	508321	Stopbar	LT	0	1	30
Westbound	508302	Advance	LT,TH,RT	185	1	7
	508306	Advance	LT,TH,RT	185	1	7
	508322	Stopbar	LT	0	1	30
Northbound	508303	Advance	LT,TH,RT	200	1	7
	508307	Advance	LT,TH,RT	200	1	7
	508311	Stopbar	LT	0	2	30
Southbound	508304	Advance	LT,TH,RT	200	1	7
	508308	Advance	LT,TH,RT	200	1	7
	508312	Stopbar	LT	0	2	30
	508328	Stopbar	RT	0	1	30
Huntington Dr&First Ave (ID: 6081)						
Traffic Direction	Detector ID	Detector Type	Detected Movements	Distance To Stopbar(ft)	Number Of Lanes	Detector Length(ft)
Eastbound	608102	Advance	LT,TH,RT	200	1	7
	608106	Advance	LT,TH,RT	200	1	7
	608114	Stopbar	LT	0	1	55
Westbound	608101	Advance	LT,TH,RT	200	1	7
	608105	Advance	LT,TH,RT	200	1	7
	608113	Stopbar	LT	0	1	55
Northbound	608104	Stopbar	LT	0	1	30
	608108	Stopbar	TH,RT	0	1	30
Southbound	608103	Stopbar	LT	0	1	30
	608107	Stopbar	TH,RT	0	1	30
Huntington Dr&Second Ave (ID: 6082)						
Traffic Direction	Detector ID	Detector Type	Detected Movements	Distance To Stopbar(ft)	Number Of Lanes	Detector Length(ft)
Eastbound	608217	Advance	LT,TH,RT	190	1	7
	608219	Advance	LT,TH,RT	190	1	7
	608214	Stopbar	LT	0	1	30
	608202	Stopbar	TH	0	1	30
	608206	Stopbar	RT	0	1	30
Westbound	608201	Advance	LT,TH,RT	190	1	13
	608205	Advance	LT,TH,RT	190	1	13
	608213	Stopbar	LT	0	1	30
	608209	Stopbar	TH	0	2	30
Northbound	608203	Advance	LT,TH,RT	180	1	7
	608207	Advance	LT,TH,RT	180	1	7
	608223	Stopbar	LT	0	1	30
Southbound	608204	Advance	LT,TH,RT	180	1	7
	608208	Advance	LT,TH,RT	180	1	7
	608224	Stopbar	LT	0	1	30

[1] “LT”, “TH”, and “RT” stand for “Left Turn”, “Through”, and “Right Turn” movements, respectively;
[2] “Distance To Stopbar” and “Detector Lengths” are measured from street views in Google Maps. Detectors at certain approaches are not observable. Therefore, the corresponding values are filled with the ones in the opposite direction, assuming a “symmetric” design.

Table 2 Signal timing plans at the three intersections.

Huntington Dr&Santa Anita Ave (ID: 5083)										
Plan Name	Activation Time	Cycle (sec)	Phase 1&5		Phase 2&6		Phase 3&7		Phase 4&8	
			G (sec)	Y+R (sec)	G (sec)	Y+R (sec)	G (sec)	Y+R (sec)	G (sec)	Y+R (sec)
E	0:00-6:00 & 21:00-24:00	110	20	3	27	5	20	3	27	5
P_1	9:00-15:30 & 19:00-21:00	120	15	3	39	5	14	3	36	5
P_2	6:00-9:00	120	11	3	46	5	11	3	36	5
P_3	15:30-19:00	120	15	3	41	5	12	3	36	5
Huntington Dr&First Ave (ID: 6081)										
Plan Name	Activation Time	Cycle (sec)	Phase 1&5		Phase 2&6		Phase 3&7		Phase 4&8	
			G (sec)	Y+R (sec)	G (sec)	Y+R (sec)	G (sec)	Y+R (sec)	G (sec)	Y+R (sec)
E	0:00-6:00 & 21:00-24:00	90	20	3	28	4	NA	NA	31	4
P_1	9:00-15:30 & 19:00-21:00	120	10	3	74	4	NA	NA	25	4
P_2	6:00-9:00	120	10	3	74	4	NA	NA	25	4
P_3	15:30-19:00	120	10	3	74	4	NA	NA	25	4
Huntington Dr&Second Ave (ID: 6082)										
Plan Name	Activation Time	Cycle (sec)	Phase 1&5		Phase 2&6		Phase 3&7		Phase 4&8	
			G (sec)	Y+R (sec)	G (sec)	Y+R (sec)	G (sec)	Y+R (sec)	G (sec)	Y+R (sec)
E	0:00-6:00 & 21:00-24:00	90	20	3	27	5	NA	NA	30	5
P_1	9:00-15:30 & 19:00-21:00	120	15	3	67	5	NA	NA	25	5
P_2	6:00-9:00	120	10	3	72	5	NA	NA	25	5
P_3	15:30-19:00	120	20	3	62	5	NA	NA	25	5

[1] "G", "Y", and "R" stand for "Green Time", "Yellow Time", and "All Red Time", respectively.
[2] The green times provided in the table are the maximum ones from the controller settings.

2.4.3 Data Source

As a continuing effort in the I-210 Connected Corridors project, we have been retrieving detector data from Arcadia's TCS server. The data used in this study was collected from 2016-01-01 to 2017-06-30. It contains a number of measurements at the interval of five minutes, e.g., hourly volume, occupancy, speed, number of stops, and delay. But we only use the measurements of hourly volume and occupancy in this study because they are direct measurements from the detectors. For the collected data, it is divided into two subsets that will be used in Section 2.6: (i) a calibration set that contains data from 2016-01-01 to 2016-12-31; and (ii) a validation set that contains the data from 2017-01-01 to 2017-06-30.

2.5 Analysis of Flow-Occupancy Relations

Before calibrating and validating the proposed trapezoidal fundamental diagram, we would like to analyze the flow-occupancy relations at both advance and stopline detectors in this section. In particular, we are interested in understanding the reliability of flow and occupancy measurements as well as how the distance to the stopline would reduce or even eliminate the impact of signal control on the traffic.

2.5.1 Flow-Occupancy Relations From the Field

As an example, we consider detectors in the eastbound approach at the intersection between Huntington Dr and Second Ave. In Figure 8, we provide the flow-occupancy plots of advance detector 680219 and stopline detector 608202 on Thursdays. The data points are marked differently according to the six activation time periods in Table 2.

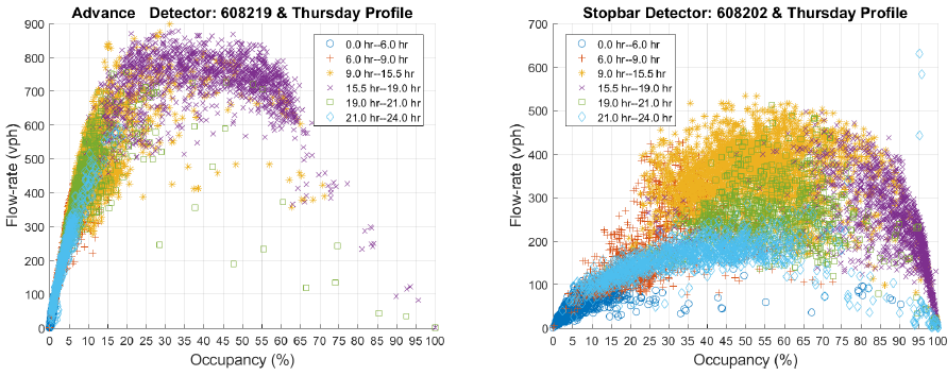

(a) Advance detector (b) Stopbar detector

Figure 8 Flow-occupancy plots on Thursdays in Year 2016

2.5.1.1 Advance Detectors

From Figure 8(a), we can find that:

(i) The maximum flow rate is attained at about 850 veh/hr/ln during the afternoon peak period, from 15:30 to 19:00. During that period, the cycle length is 120 seconds, and the green time is 62 seconds. If we consider vehicle's lost time is close to the yellow and all red time, the effective green ratio is about 0.52. Furthermore, if we consider the saturation flow rate is about 1700 veh/hr/ln, the observed maximum flow rate is very close to the capacity in this direction, which is about 884 veh/hr/ln.

(ii) The upper bound of the flow-occupancy plot turns out to be trapezoidal with two break points, which is very consistent with the proposed one in Figure 1.

(iii) There are scattering points below the trapezoidal upper bound. There are several potential reasons for this. The first reason is the lack of upstream demand. If the demand is lower than the capacity, we should expect the points are below the upper bound. The second reason is poor coordination between intersections. In such a case, vehicle platoons exiting from the upstream intersection may frequently hit the red phase of the downstream intersection. If the demand is high enough, it is possible to form a queue that reaches the location of advance detectors, which as a result generates high occupancies and flow rates. The third reason is the existence of initial queue due to the lack of green time or downstream congestion. For example, if downstream traffic is congested, which limits vehicle passages at the intersection, a queue will form and propagate to the advance detectors. Similarly, if the upstream arrival rate is low but there is an initial queue at the intersection approach, such a queue will persist and may reach the advance detectors if the green time is too short to clear all vehicles within a cycle. As a result, the flow-rate at the advance detectors is low, while the corresponding occupancy is high.

2.5.1.2 Stopline Detectors

From Figure 8(b), we can find that the flow-occupancy relation is significantly different from that in Figure 8(a). First of all, the data points are scattering in a wider range in the flow-occupancy space. Second, the whole curve is skewed to the right, yielding a lower slope of the upper bound on the left-hand side. Third, more points with lower flows and higher occupancies are observed. Particularly, we observe traffic is totally blocked with 100% occupancy for certain time periods. This significant difference between Figure 8(a) and Figure 8(b) may be due to the fact that stopline detectors are more impacted by signal control. Even though vehicle platoons can pass the upstream advance detectors without stopping, they may hit the red light at different time stamps and wait for the next green phase. Also, vehicles at the stopline detectors are directly impacted by downstream traffic conditions, e.g. queue spillback. In addition, driver's behaviors may vary when they approach the stopline, which also contributes to the wide scattering of data points.

2.5.2 Advantages of Advance Detectors

In the following, we further analyze the reliability of flow count measurements as well as the impact of distance to the stopline so as to demonstrate the advantages of using data from advance detectors.

2.5.2.1 Reliability of Flow Count Measurements

In Figure 6, there is full detector coverage in the eastbound direction at the intersection between Huntington Dr and Second Ave. The upstream includes two advance detectors, 608217 and 608219, while the downstream includes three stopline detectors, 608214 for left turn, 608202 for through, and 608206 for right turn. In Figure 9, we provide the check of flow conservation among these detectors. As shown in Figure 9(a), when traffic is not congested, flow conservation generally holds between the upstream and the downstream detectors. However, when traffic is congested, flow conservation doesn't hold, which can be observed from Figure 9(b). The main reason is because stopline detectors normally have longer detection lengths. As a result, they will undercount vehicle volumes when traffic is very congested with small gaps between consecutive vehicles. Therefore, flow counts from stopline detectors are less reliable than those from advance detectors.

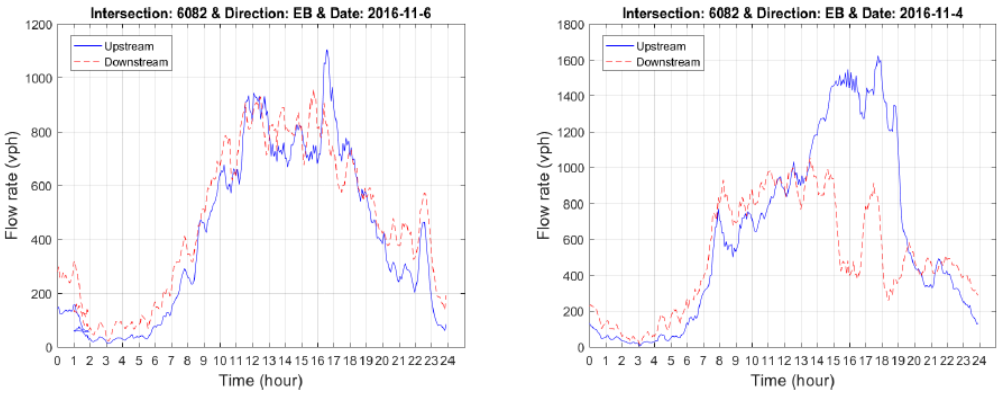

(a) On Sunday (b) On Friday

Figure 9 Flow conservation check in the eastbound direction of Huntington Dr&Second Ave.

2.5.2.2 Impact of Distance to the Stopline

From Figure 8, we can clearly see that data points from the stopline detectors are scattering at a wider range, thus we are not able to see a clear relationship between flow and occupancy. Therefore, we further analyze how the distance to the stopline will reduce, or even eliminate the impact of signal control. In order to do this, we use microsimulation in AIMSUN[2]. We create a simple network in AIMSUN, which is provided in Figure 10(a). The demands are only created to allow vehicles going from Point A to Point B. The demands gradually increase over time so as to generate different queuing profiles at the approach where the targeted detectors are located. Furthermore, in order to general queue spillback to reduce the outflow rates at the stopline, we create an activation point at Point B, the outflow rate of which gradually reduces over time. Under the same OD demands, signal settings, and boundary constraints, detectors are installed every 50ft from the stopline, from 1.5ft to a maximum of 200ft. The corresponding flow-occupancy plots are provided in Figure 10(b) to (f), respectively. From the figures, as detectors are shifting away from the stopline, it is clear to see that: (i) flow rates increase at the points with low occupancy; (ii) data points are less scatting in the flow-occupancy space, and thus a better shape can be observed; and (iii) no significant differences are observed from the flow-occupancy plots when the distance is over 150ft. Therefore, in order to reduce the signal impact, it is better to use data from advance detectors.

[2] https://www.AIMSUN.com/. We have verified AIMSUN is able to replicate driver's behaviors and generate flow and occupancy plots consistent with the field data. But we omit the analysis here since it is irrelevant.

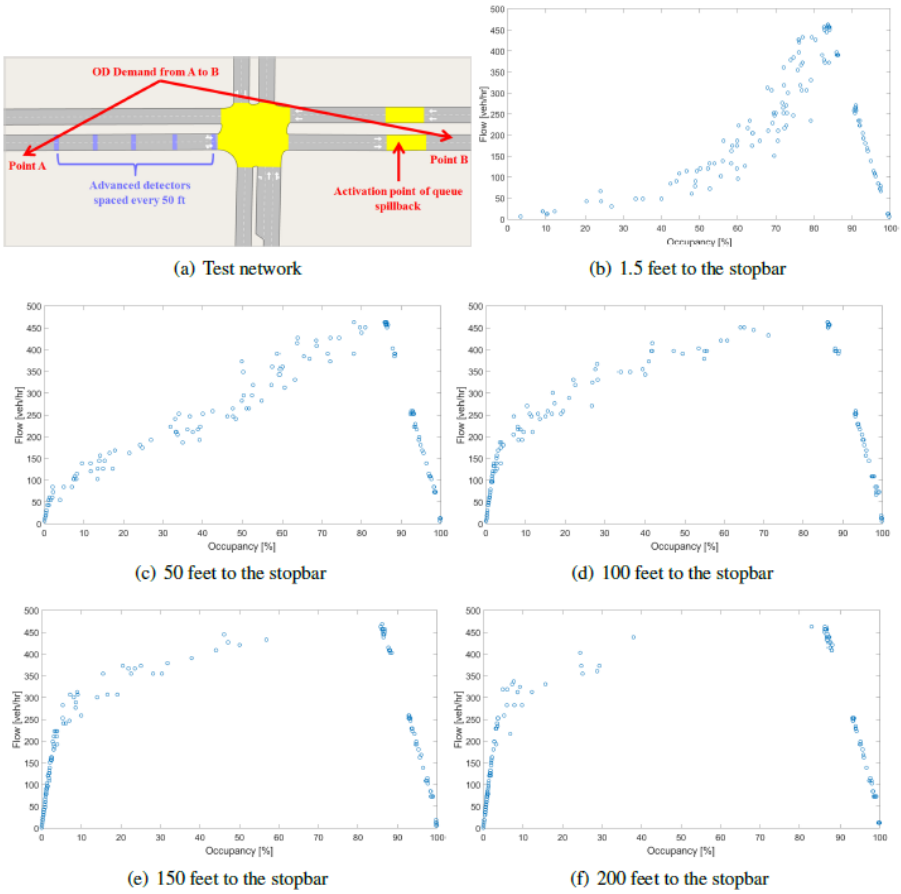

(a) Test network (b) 1.5 feet to the stopbar

(c) 50 feet to the stopbar (d) 100 feet to the stopbar

(e) 150 feet to the stopbar (f) 200 feet to the stopbar

Figure 10 Flow-occupancy plots from detectors with various distances to the stopline.

2.6 Calibration and Validation

In this section, we focus on the calibration and validation of the proposed trapezoidal fundamental diagram in Section 2.2 using data from advance detectors in the study site.

2.6.1 Calibration

In order to derive the trapezoidal fundamental diagram in Equation 8, the following parameters should be known/estimated first:

(i) Detector length D;

(ii) Averaged vehicle length L;

(iii) Saturation speed v_s;

(iv) Cycle length C;

(v) Green time G;

(vi) Saturation flow rate q_s (or equivalently, saturation headway h_s).

For detector length D, it varies a lot depending on its configuration. For example, for advance detectors, the length is about 7 feet if they are "single-loop", while it is about 13 feet if they are "dual-loop". In reality, detector length can be measured from the field using street view in Google Maps. Examples can be found in Table 1. For vehicle length L, its average is about 17 feet for regular automobiles (Cheung et al., 2005). For saturation speed $\mathrm{v_s}$, we can use the posted speed limit instead, considering drivers do not violate the traffic rule. For example, the speed limit along Huntington Dr is 30mph, while it is 35mph along Santa Anita Ave and Second Ave. For cycle length C, it can be obtained directly from the traffic system. Especially, when it is under signal coordination, a common cycle length will be used. Examples can be found in Table 2.

For the estimation of green times, it is a little complicated since it is closely related to the signal phase settings. In our study, we use the maximum green time among the traffic movements at a given approach, which normally is the green time for through and right-turn movements. The reasons to use this maximum value are:

(i) If all traffic movements share the same phase, e.g., Phases 4 and 8 for the southbound and northbound in Figure 7(b) and Figure 7(c), the maximum green time is the actual allocated one for this phase. In this case, the estimation is correct.

(ii) If the left turns for the E-W or the N-S directions are "protected" and under the setting of "Lead-Lag" phasing, the maximum green time is the one for the through and right turn movements, which is also the actual/maximum green time allocated to that approach. Therefore, the estimation is also correct.

(iii) If the left-turns for the E-W or the N-S directions are "protected" and under the setting of "Lead-Lead" phasing, e.g., the left-turn settings for the E-W directions in Figure 7, the maximum green time would be the one allocated to the through and right-turn movements. In such a case, the green time is a little bit underestimated since some left-turn vehicles can pass the advance detectors during the allocated green time. As a result, the capacity for the given approach will be underestimated. However, this error won't be significant if the left-turn arrival rate is relatively low.

Therefore, the most important part is to estimate the saturation flow rate (or equivalently, the saturation headway). Suppose we have a set of M flow-occupancy data points, i.e.,$\{q_i\}$ and $\{Occ_i\}$, and the corresponding green times $\{G_i\}$ and cycle lengths $\{C_i\}$, for $i \in [1, M]$. From Figure 8(a), there is a wide range of occupancy where the flow rates are almost constant. Therefore, we can select the data points in this region to estimate the saturation flow rate. After collecting enough data points, e.g., for several months, we estimate the saturation flow rate using the procedure in Algorithm 1.

Algorithm 1 Estimation of the saturation flow rate

for Each advance detector **do**
  Collect a subset of data points belonging to the same signal control plans in Table 2.
  for Each signal control plan **do**
    Define the occupancy region $[Occ_{min}, Occ_{max}]$.
    Select a subset of data points if their occupancies are within the defined range.
    if the subset size is less than $N_{threshold}$ **then**
      Use a default value, $q_s = 1800$veh/hr/ln, or equivalently, $h_s = 2.0$s.
    else
      For the subset $\{Occ_j\}$, $\{q_j\}$, $\{G_j\}$, and $\{C_j\}$, for $j \in [1,N]$ and $N \leq M$, use Equation 10 to recalculate the saturation flow rates $\{q_s^j\}$.
      Choose q_s as the β percentile of the estimated $\{q_s^j\}$.
    end if
  end for
end for

$$q_s^j = q_j \times \frac{C_j}{G_j}. \tag{9}$$

In this study, we set Occ_{min} = 0.20 (or 20%) and Occ_{max} = 0.55 (or 55%). In order to have enough data points in each subset, we set $N_{threshold}$ = 1 data point × number of days used. That means we require daily traffic congestion should last for at least 5 minutes. Instead of using the maximum value of $\{q_s^j\}$, we set β = 95 to give enough margin to avoid outliers.

For calibration, the whole year flow and occupancy data in 2016 in our study site is used. All advance detectors are considered except Detectors 608204 and 608208 because they were failed in the year of 2016. Therefore, we have a total of 18 advance detectors in our study site. For a given point of flow and occupancy, e.g., (Occ_j,q_j), we obtain its corresponding green time and cycle length, e.g., (G_j, C_j), by checking its time interval and the signal timing plans provided in Table 2. Actually, it is not necessary to get the exact green time for a particular point of flow and occupancy. The reason is if the green time is not fully used, the corresponding flow rate would be lower than the capacity. If we replace the actual green time with the planned one, which is a larger value in the denominator in Equation 10, the estimated saturation flow rate is even lower and will be directly eliminated since we are using the percentile instead of other measurements (e.g., mean value).

In Table 3, we provide the estimated saturation flow rates under different control plans for the 18 advance detectors in our study site. We use a default saturation flow rate for those periods without enough data, which are highlighted in red in Table 3. Examples on how to estimate the saturation flow rate are provided in Figure 11. From the table, we find that

(i) The estimated saturation flow rate varies a lot among detectors as well as control plans. For example, the highest saturation flow rate reaches 2316 veh/hr/ln at Detector 508303 under the control plan P_2, while the lowest one reaches 1179 veh/hr/ln at Detector 608205 under the control plan P_2.

(ii) It is not possible to estimate the saturation flow rate for the control plan E due to the fact that traffic is not congested during the activation time period. Therefore, a default saturation flow rate of 1800 veh/hr/ln is used.

Table 3 Estimated saturation flow rates at the three intersections

Intersection	Direction	Detector ID	q_s (veh/hr/ln)			
			E (Evening)	P_1 (Off-Peak)	P_2 (AM Peak)	P_3 (PM Peak)
Huntington & Santa Anita	EB	508301	1800	2127	1800	2107
		508305	1800	2047	1800	1992
	WB	508302	1800	2036	2073	1800
		508306	1800	2020	2127	1862
	NB	508303	1800	2190	2316	1994
		508307	1800	2171	2272	1971
	SB	508304	1800	1320	1290	1376
		508308	1800	1231	1248	1303
Huntington & First	EB	608102	1800	1800	1800	1330
		608106	1800	1237	1800	1313
	WB	608101	1800	1800	1800	1800
		608105	1800	1800	1325	1800
Huntington & Second	EB	608217	1800	1800	1800	1577
		608219	1800	1466	1800	1616
	WB	608201	1800	1568	1362	1435
		608205	1800	1800	1179	1800
	NB	608203	1800	1800	2064	1800
		608207	1800	1800	1800	1800

Note: A default saturation flow rate (highlighted in red), 1800 veh/hr/ln, is used for those periods without enough data.

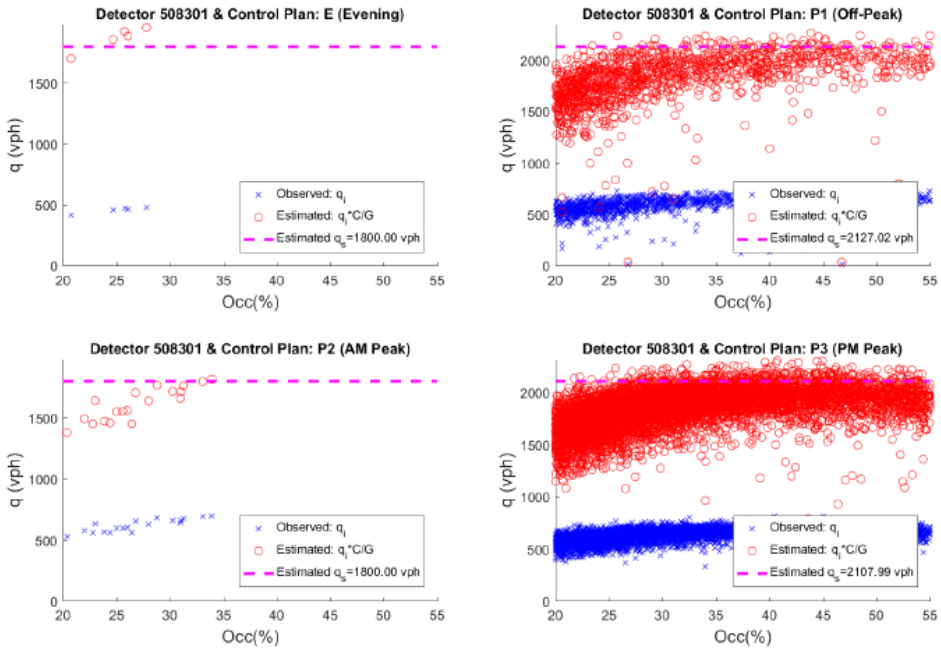

Figure 11 Examples of estimated saturation flow rates: Eastbound at Hunting Dr&Santa Anita Ave.

Furthermore, we check the network and signal settings carefully and find the following aspects that can lead to low saturation flow rates.

(i) Inappropriate detector placement. In the southbound of Huntington Dr&Santa Anita Ave, the two advance detectors, i.e., 508304 and 508308, are placed at the buffer area where two upstream lanes are further divided into two downstream lanes, two left-turn lanes, and one right-turn lane. As a result, some vehicles may escape from the detection, which leads to low saturation flow rates estimated from the data (See Figure 12).

(ii) Shared lanes by multiple traffic movements. In the eastbound and westbound of Huntington Dr&First Ave, the rightmost lane is shared by the through and right-turn movements (See Figure 6). As a result, the outflow rates at the four advance detectors, i.e., 608101, 608102, 608105, and 608106, are lower due to the slow-moving right-turn vehicles. Also, we have checked the historical signal timing data and find that Pedestrian Call is often activated at this intersection, which as a result leads to even lower saturation flow rates (See Figure 13).

(iii) Temporary lane blockages by left-turn and right-turn movements. When Pedestrian Call is activated, left-turn and right-turns vehicles may have to wait before the intersection is clear to cross. As a result, it may create temporary lane blockages to reduce the outflow rate in the upstream section where advance detectors are often located. In such a case, we also expect low saturation flow rates.

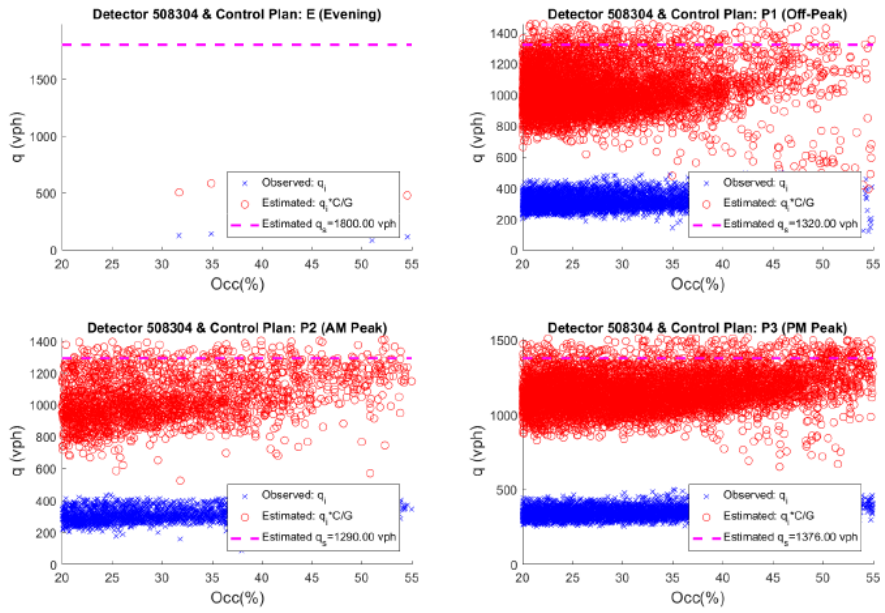

Figure 12 Examples of estimated saturation flow rates: Southbound at Hunting Dr&Santa Anita Ave.

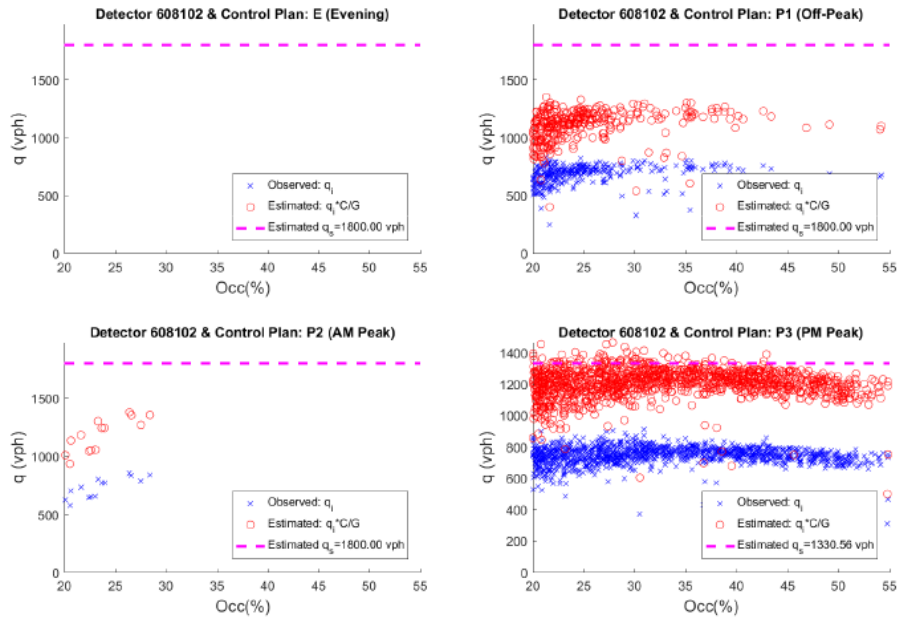

Figure 13 Examples of estimated saturation flow rates: Eastbound at Hunting Dr&First Ave.

2.6.2 Validation

In this subsection, we only validate the estimated trapezoidal fundamental diagrams for those detectors and control plans with estimated saturation flow rates available in Table 3. Herein, the first six-month (from January to June) flow and occupancy data in 2017 is used for validation. Before that, we follow the procedure in Algorithm 2 to get the upper bound of flow-occupancy plots, which is considered to represent the actual trapezoidal fundamental diagrams.

Algorithm 2 Derivation of the upper bound of the flow-occupancy plots

for Each advance detector **do**
  Collect a subset of data points belonging to the same signal control plans in Table 2.
  for Each signal control plan **do**
    Divide the occupancy region $[0, 1]$ into K small bins with a step size of Δ.
    Assign the flows $\{q_i\}$ into the corresponding bins according to the occupancies $\{Occ_i\}$.
    for Each bin k with size M_k greater than the threshold N_Δ **do**
      The occupancy $\bar{Occ}_k$ is taken as the mean observation $\frac{\sum_{i=1}^{M_k} Occ_i}{M_k}$.
      The flow rate $\bar{q}_k$ is taken as the β percentile of the total observations.
    end for
  end for
end for

For the parameters in Algorithm 2, we set Δ= 0.02, which leads to a maximum of 50 bins. In order to maximize the chance of having data points reaching the actual upper bound, we set N_Δ = 10 based on the current setting of Δ and the given number of days in the validation dataset. To avoid potential outliers, we set β = 95 instead of using the maximum observation inside each bin.

For detector d and signal control plan s, we can get the estimated trapezoidal traffic flow fundamental diagram, i.e., $q = Q_{d,s}^{est}(Occ)$. Using the procedure in Algorithm 2, we also can get the upper bound of the flow and occupancy data, i.e., $\{\bar{q}_k\}$ and $\{\overline{Occ}_k\}$ for $k \in [1, \bar{K}]$ and $\bar{K} \leq K$. To assess estimation accuracy, the MAPE is used and is computed as below:

$$\boldsymbol{MAPE} = \frac{\mathbf{100}}{\bar{\boldsymbol{K}}} \sum_{\boldsymbol{k=1}}^{\bar{\boldsymbol{K}}} \left| \frac{\boldsymbol{Q_{d,s}^{est}(\overline{Occ}_k) - \bar{q}_k}}{\bar{\boldsymbol{q}}_{\boldsymbol{k}}} \right|. \quad \textbf{(10)}$$

We provide two examples of validation results in Figure 14. Figure 14(a) illustrates a good case at Detector 608219 with control plan P_3. As shown in the figure, the estimated upper bound covers all three regions: Uncongested, Congested, and Downstream spillback, and the estimated trapezoidal fundamental diagram matches the upper bound very well with a MAPE of 6%. Figure 14(b) illustrates a bad case at Detector 508302 with control plan P_2. From the figure, we can find that when traffic is uncongested, e.g., with Occ < 10%, the estimated trapezoidal fundamental diagram matches the upper bound very well. However, as traffic gets congested, the observed data points are shifted to the right with the same flow rates but higher occupancies, and therefore, significant differences are observed between the upper bound and the estimated trapezoidal fundamental diagram. Such a pattern indicates that upstream vehicle platoons often arrive at the intersection approach during the red time period and have to wait for the next green phase, which as a result leads to extra waiting times and higher occupancies.

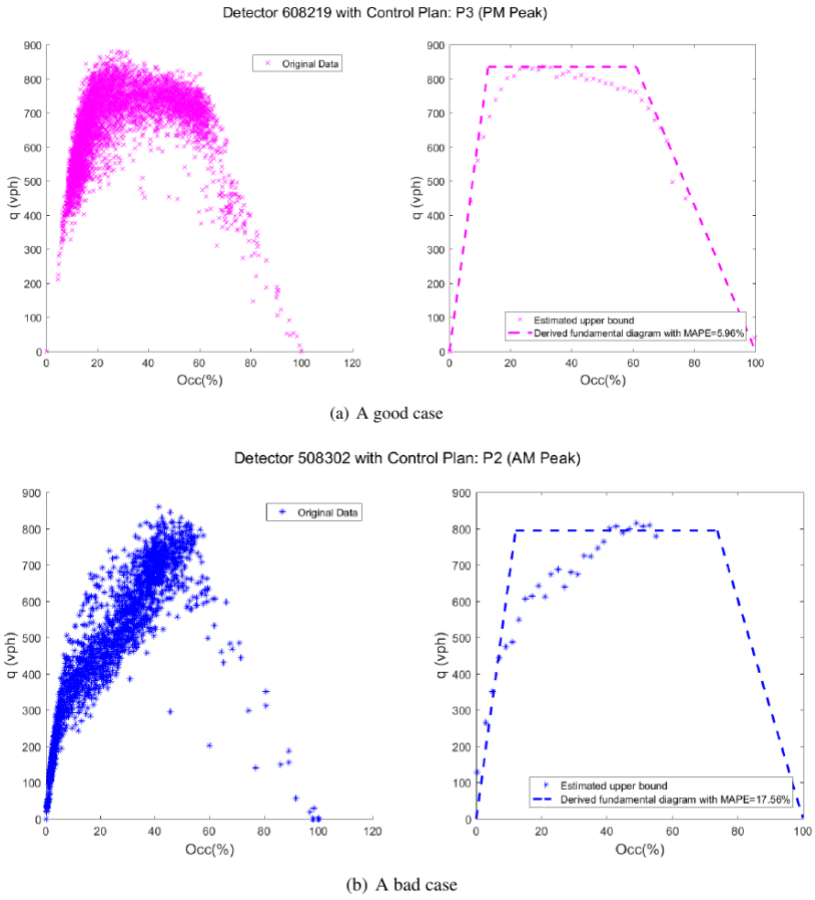

Figure 14 Examples of validation results.

In Table 4, we provide the validation results for the estimated trapezoidal fundamental diagrams at the study site. From the table, we find that:

(i) The estimated trapezoidal fundamental diagram generally matches the estimated upper bound well. Particularly, all the MAPEs under control plan P_3 and most of the MAPEs under control plan P_2 are less than 15%.

(ii) The validation results vary among intersections and approaches. For example, the MAPEs are higher at Huntington Dr&Santa Anita Ave, particularly for the eastbound and westbound directions.

(iii) The validation results vary among control plans. For example, the average MAPE for P_1 is the highest (17.2%), while the one for P_3 is the lowest (7.77%).

Table 4 Validation results for the estimated trapezoidal fundamental diagrams.

Intersection	Direction	Detector ID	MAPE (%)			
			E (Evening)	P_1 (Off-Peak)	P_2 (AM Peak)	P_3 (PM Peak)
Huntington & Santa Anita	EB	508301	N/A	19.405	N/A	14.663
		508305	N/A	24.749	N/A	13.887
	WB	508302	N/A	42.897	17.564	N/A
		508306	N/A	18.825	18.510	13.075
	NB	508303	N/A	8.376	6.484	3.367
		508307	N/A	8.319	6.801	4.363
	SB	508304	N/A	16.866	11.960	8.315
		508308	N/A	8.405	14.625	7.145
Huntington & First	EB	608102	N/A	N/A	N/A	3.492
		608106	N/A	14.447	N/A	4.408
	WB	608101	N/A	N/A	N/A	N/A
		608105	N/A	N/A	12.486	N/A
Huntington & Second	EB	608217	N/A	N/A	N/A	5.277
		608219	N/A	7.391	N/A	5.956
	WB	608201	N/A	19.474	16.011	9.267
		608205	N/A	N/A	13.085	N/A
	NB	608203	N/A	N/A	13.965	N/A
		608207	N/A	N/A	N/A	N/A
Average Value			N/A	17.196	13.149	7.768

In reality, high MAPEs in Table 4 may be caused by the following aspects.

(i) The lack of enough data points. Even though we have set a threshold for each bin, still it is not quite clear how many data points are enough to have a higher chance to reach the actual trapezoidal fundamental diagram.

(ii) Poor coordination level. As we have illustrated in Section 2.3.3, for a given arrival rate, poor coordination level can lead to high occupancies. If offsets at the upstream intersections are not set appropriately, it is possible to have vehicle platoons always arrive during the red time period. As a result, we are not able to observe the upper bound no matter how many points we have collected from the field.

Nevertheless, according to the validation results in Figure 14 and Table 4, we conclude that the trapezoidal fundamental diagram does exist in the field, and the derivation proposed in this study is valid under various settings of road geometries and signal control plans.

2.7 Discussion

A general approach is proposed to estimate the trapezoidal fundamental diagram for arterial road links using data from advance loop detectors. Under the assumption of platoon arrivals with no dispersion, the break points in the trapezoidal fundamental diagram are derived using the information from road geometries, detector layout, signal settings, and vehicle dynamics. We pointed out that the proposed trapezoidal fundamental diagram is point-based, which represents most of the traffic states on a link. However, when traffic is very congested and the residual queue spills over the advance detectors, it fails to represent the actual queue length on the link. Furthermore, we analytically demonstrated that with minor dispersion, our estimation

of vehicle waiting time at advance detectors is accurate. We also graphically showed that under near-stationary traffic states the impact of initial queue can be ignored. However, poor coordination level will degrade the traffic performance, shifting the data points to the right with higher occupancies. Three intersections along Huntington Drive in the City of Arcadia were selected as a test site. Detector data was collected for one year and a half and was divided into two subsets: the first 12 months for calibration, and the rest for validation. According to the flow-occupancy plots at both stopline and advance detectors, we found that it is better to use data from advance detectors since measurements from stopline detectors are significantly impacted by the traffic signal and are not reliable under severe congestion. In order to obtain the trapezoidal fundamental diagram, we estimated the saturation flow rates at different advance detectors under different signal control plans using the calibration dataset. We found that the saturation flow rate varies a lot among intersection approaches as well as signal control plans. Low saturation flow rate may be caused by a number of aspects, for example, inappropriate detector placement, shared lane with multiple traffic movements, active pedestrian activities, and temporary lane blockages by the turning movements. Furthermore, using the validation dataset, we estimated the upper bounds of flow-occupancy plots, which is considered to represent the actual fundamental diagrams. Then we calculated the corresponding MAPEs against with the estimated trapezoidal fundamental diagrams. We demonstrated that the estimated trapezoidal fundamental diagram generally matches the field data well, which in turn proves the existence of such a fundamental diagram on arterial road links.

3. Part III: Arterial Traffic State Estimation

3.1 Problem Statement

Traffic estimation plays a key role in the Decision Support System (DSS) in Integrated Corridor Management (ICM). For traffic management agencies, arterial traffic estimation is most needed when traffic incidents occur on freeways since they need to ensure the recommended response plans do not detour freeway traffic to the arterial road links that are already congested. In the literature, there have been studies that estimate traffic queues using data in a fine granularity, e.g., event-based (Liu et al., 2009) or 30 seconds (Skabardonis and Geroliminis, 2008). However, conventional controllers will aggregate and report traffic data in longer intervals, e.g., five minutes, and therefore, the proposed methods in the aforementioned studies won't work. Moreover, when traffic prediction is used in the DSS, it is very important to make sure the network starts with a set of "reasonable" traffic states, particularly at active bottleneck locations. The state-of-the-practice approach is to use a warm-up period to load appropriate numbers of vehicles into the network under given demand and control settings. However, due to the complexity in road geometry and the uncertainty in simulation inputs, it is very difficult to drive initial traffic states to the correct ones for arterial networks. Also, the warm-up period becomes significantly longer as the size of the network gets bigger, as is the network size of the I-210 Connected Corridors Pilot. Therefore, a more direct approach is needed to use the conventional traffic data to estimate the traffic states in arterial networks.

With the existence of signal control, traffic in arterial networks is very different from that on freeways. For a given intersection approach, different vehicle movements interact with each other, especially when traffic is congested. A severe condition is the occurrence of lane blockage and queue spillback when the upstream demand of a particular movement is higher than the allocated capacity and persists for a long time. To evaluate intersection performance, metrics of delay and LOS are usually used. However, the prevailing HCM method (TRB, 2000) that is used to compute delay and LOS is not reliable under heavy traffic congestion (Gan et al., 2017), particularly when lane blockage or queue spillback occurs. Therefore, instead of using indirect measurements of delay and LOS, it would be extremely helpful if we can directly estimate the traffic states at individual intersection approaches to assess the overall performance.

In this part, we aim to tackle the problems discussed above. In Part II, we have developed occupancy thresholds to categorize detector data into different regimes/states at advance and stopline detectors. Therefore, we first perform a fitness analysis of the proposed occupancy thresholds using data from the field and microsimulations. Then we develop an estimation algorithm that fuses data from advance and stopline detectors with signal phasing information from the field. The estimation output consists of traffic states and average queues for the traffic movements at an intersection approach. The proposed estimation algorithm is generic since we consider various combinations of road geometry, detector layout, and signal setting in the field and we try to maximize the amount of detail given the availability and quality of the detector data. Under the assumptions of congested traffic and minor turning movements, we theoretically prove there exists a linear relation between the total vehicle queues and the travel times at multiple intersections along an arterial corridor. We further select five intersections along Huntington Dr. in the City of Arcadia as a test site and validate such a linear relation for the eastbound and the westbound traffic. In addition, we propose a general framework of traffic initialization in the microsimulation software, AIMSUN. We develop an initialization algorithm that generates simulated vehicles from the estimated traffic queues and the detailed network structure in AIMSUN. As an application example, we apply the proposed framework to the I-210 AIMSUN model and initialize the traffic states in the City of Arcadia. The proposed framework in this part is novel, which provides a fundamentally different way of state estimation and initialization. It is expected to outperform the conventional method given good detector coverage and data quality.

3.2 Fitness Analysis of Occupancy Thresholds at Advance and Stopline Detectors

In Section 2.2.3, two occupancy thresholds (i.e., Occ_1^{adv} and Occ_2^{adv}) are proposed to determine traffic states at advance detectors, i.e., Equation 4 and Equation 5. According to these two thresholds, we can further divide the flow-occupancy plots into three regimes:

(i) Uncongested regime with $Occ \leq Occ_1^{adv}$;

(ii) Congested regime with $Occ_1^{adv} < Occ \leq Occ_2^{adv}$;

(iii) Downstream spillback regime with $Occ_2^{adv} < Occ \leq 1$.

From Figure 8(b), we can clearly see that the flow-occupancy plot at stopline detectors is significantly different from the one at advance detectors, with points scattering in a wider region. The major reason for this is the signal control. Although vehicle platoons can pass advance detectors without stopping, they may be forced to stop behind the stopline due to the activation of red light. Depending on the waiting time on red, there exists infinitely many occupancies at a given flow rate. Therefore, the first occupancy threshold in Equation 4 is not applicable to stopline detectors.

However, when the number of upstream queued vehicles is high enough, the allocated green time will be fully used once it is activated. Depending on the occurrence of downstream queue spillback, the second occupancy threshold Occ_{stp} in Equation 5 should be applied. Also, we have observed that the occupancy measurement is more reliable than the flow measurement at stopline detectors when traffic is congested. With this occupancy threshold, the flow-occupancy domain for stopline detectors can be divided into the following regions:

(i) No downstream spillback regime with $Occ \leq Occ_{stp}$;

(ii) Downstream spillback regime with $Occ > Occ_{stp}$.

In the following, we are using both field and simulated data to perform a fitness analysis of the occupancy thresholds at advance and stopline detectors.

3.2.1 Using Field Data

In this case, we take the detectors at Huntington Dr and 2nd Ave as an example (See Figure *6*).

3.2.1.1 Advance Detectors

Since signal settings are changing over time, we select the PM peak period (15:30 hr– 19:00 hr) for analysis. At that time period, C =120s and G=62s according to Table 2. For illustration purposes, we take the advance detectors in the eastbound and westbound approaches as an example. The saturation flow rate is chosen as q_s = 1700vph, and the saturation speed is chosen as the speed limit, i.e., v_s = 30mph. We select the average vehicle length as L = 17ft, and the detector length $as\ D = 7ft$ (See Table 1), which means the effective vehicle length is $L + D$ = 24ft and the jam density is 220vpm.

In Figure 15, we provide the flow-occupancy plots with the estimated occupancy thresholds for the four advance detectors in the eastbound and westbound approaches. From the figure, it is clear to see that the two occupancy thresholds perfectly match the change points in the flow-occupancy plots, particularly for the advance detectors in the eastbound approach. In the westbound approach, traffic is not very congested and no queue spillback is observed. Nevertheless, the first occupancy threshold perfectly matches the transition from uncongested to congested regimes. Therefore, the figure supports the validity of the proposed occupancy thresholds for advance detectors.

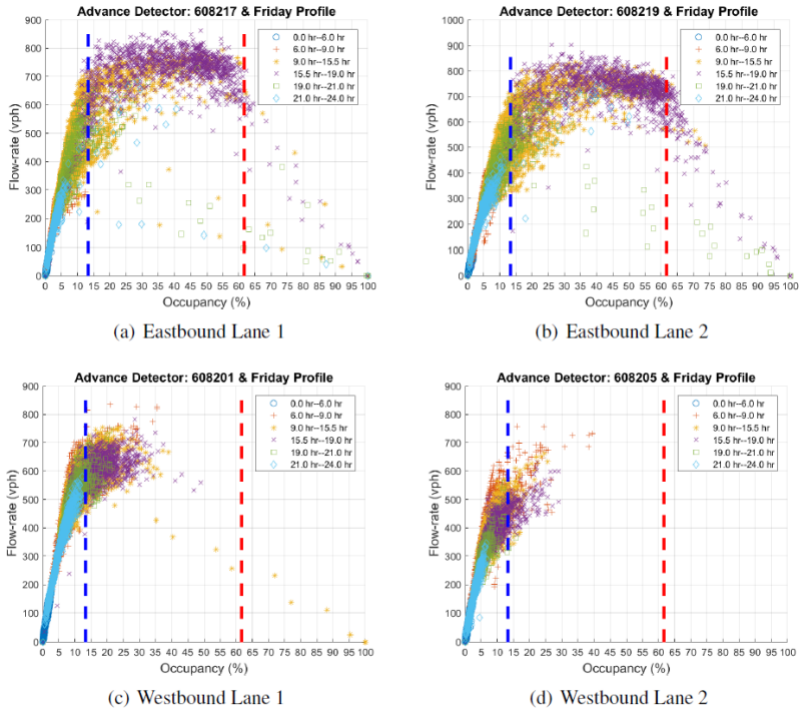

(a) Eastbound Lane 1 (b) Eastbound Lane 2

(c) Westbound Lane 1 (d) Westbound Lane 2

Figure 15 Occupancy thresholds of advance detectors at Huntington Dr and 2nd Ave.

3.2.1.2 Stopline detectors

Here, we again consider the PM peak period (15:30 hr – 19:00 hr). We focus on the stopline detectors in the eastbound and westbound approaches, particularly for those detecting left-turn and through movements. Since vehicles at the stopline must accelerate at the beginning of the green phase, we assign a lower saturation speed for the though movement, i.e., v_s^{TH} = 25mph. In addition, because left-turn vehicles are required to turn to other links, we assign an even lower speed for the left-turn movement, i.e., v_s^{LT} = 20mph. The corresponding detector lengths are obtained from Table 1. According to the signal settings in Table 2, we can calculate the occupancy threshold using the formula in Equation 5.

In Figure 16, we provide the flow-occupancy plots with the estimated occupancy thresholds for the stopline detectors in the eastbound and westbound approaches. For the eastbound through movement, it can be seen that the estimated threshold matches the data points well: the flow-rates drop when the occupancies are higher than the threshold. For the left-turn movement, we can see that the number of left-turn vehicles is very small, most likely one or two vehicles per cycle.

For the westbound through movement, we can see that the majority of the data points are on the left-hand side of the estimated threshold, which indicates that the downstream is mostly in free conditions. Such a pattern is consistent with the flow-occupancy plots in Figure 15(c) and Figure 15(d), in which queue spillback was an infrequent occurrence. For the left-turn movement,

we can see that the volume is not high, about two to three vehicles per cycle. It is very rare to see the case when downstream congestion reduces the discharging flow of left turn vehicles.

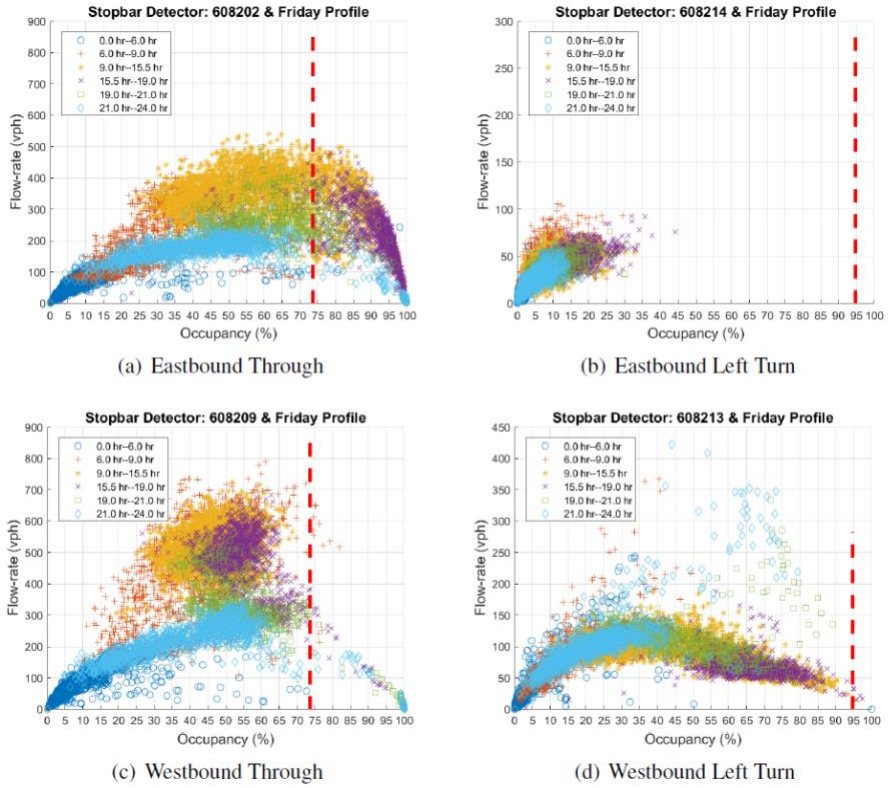

(a) Eastbound Through (b) Eastbound Left Turn

(c) Westbound Through (d) Westbound Left Turn

Figure 16 Occupancy thresholds of stopline detectors at Huntington Dr and 2nd Ave.

3.2.2 Using AIMSUN Microsimulation Model

Test Network and Experiment Setup

In AIMSUN, we create a test network to validate the flow-occupancy curves and critical occupancies. Detailed network layouts are shown in Figure 17. In order to generate queue spillback, we create a break point in the downstream road link. This break point is simply a traffic signal, which is typically set to all green so that vehicles can pass freely. When testing the case of queue spillback, the break point is activated by introducing red time to reduce the vehicle throughput.

The experiment consisted of four simulations. Because the critical occupancies depend on the green ratio $\frac{G}{C}$ of an approach, we hold all other parameters in Equations 4 and 5 constant in each simulation while only varying the green time G at the targeted ("East") intersection.

In our experiment setup, each simulation lasted for 24 hours. For simplicity purposes, we only test the performance of stopline and advance detectors in the southbound direction at the

targeted (“East”) intersection. The parameter settings provided in Table 5 are constant throughout all simulations.

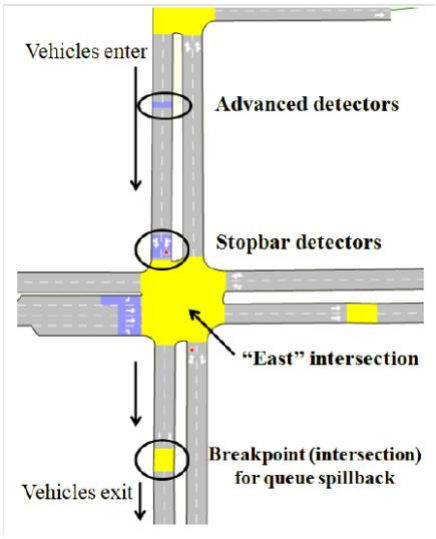

Figure 17 Test network in AIMSUN.

Table 5 Parameter settings in AIMSUN simulation.

Parameter	Definition	Value
L	Vehicle length	13.12 ft
D	Length of advance detector	5.9 ft
	Length of stopbar detector (Through and right-turn movements)	22.3 ft
	Length of stopbar detector (Left-turn movement)	38 ft
v_{sat}	Saturation speed (Advance detector)	25 mph
	Saturation Speed (Through)	20 mph
	Saturation Speed (Left turn and right turn)	15 mph
h	Saturation headway	2.3 s
C	Cycle length	90 s

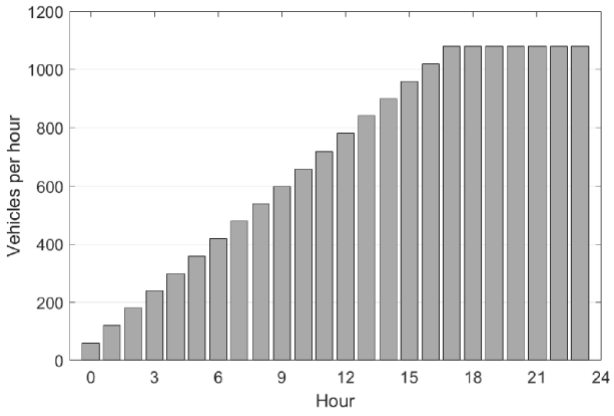

Figure 18 Demand profile over 24-hour AIMSUN simulation.

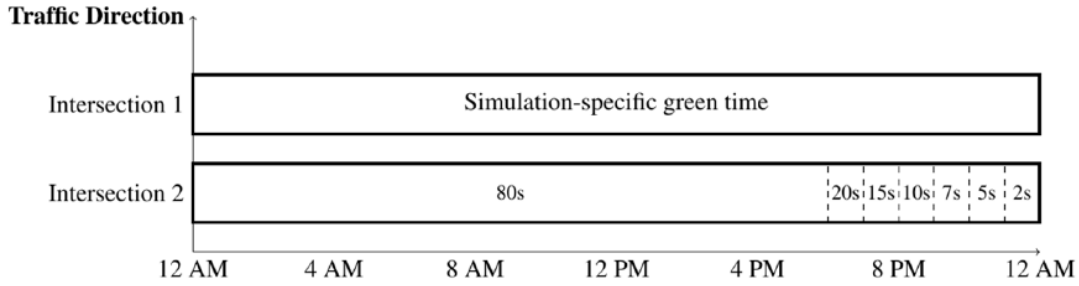

Figure 19 Signal green time settings at the two intersections.

The demand settings for traffic going from north to south is provided in Figure 18, while the signal plans for the two intersections are depicted in Figure 19. For example, Intersection 1 ("East" Intersection) in the first simulation had a constant green time of 25s for the north-to-south through movement. Meanwhile, Intersection 2 (Breakpoint Intersection)'s green time was decreased throughout the simulation according to the settings shown in Figure 19. In order to observe the derived occupancy thresholds (i.e., Occ_1 and Occ_2) from the flow-occupancy curves, each simulation is created according to the following procedures to create enough variations in traffic behavior.

(i) First, the green time G for Intersection 1 was varied between each trial to verify the dependence of advance detector's critical occupancies on the signal plan. Four trials were created, with green times of 25s, 20s, 15s, and 10s.

(ii) Second, from 12 AM - 5 PM the demand is increasing linearly from 60vph to 1080vph, with the green time in Intersection 2 held constant. This creates traffic conditions that form the regimes of "uncongested" and "congested" without spillback.

(iii) Third, while keeping the demand constant, from 5 PM - 12 AM the green time in Intersection 2 decreases each hour to create different amounts of queue spillback.

Note that the demand and signal settings are set arbitrarily, which definitely does not reflect any traffic patterns (e.g., AM and PM peaks) observed in the field.

3.2.2.1 Experiment results

For advance detectors, we calculate the occupancy thresholds using Equations 4 and 5: the first critical occupancy $\mathrm{Occ}_1^{\mathrm{adv}}$ marks the transition between the uncongested and congested without spillback regimes, while the second occupancy $\mathrm{Occ}_2^{\mathrm{adv}}$ marks where spillback begins within the congested traffic portion. For stopline detectors, only one occupancy threshold is used to determine whether there exists downstream queue spillback or not, which is calculated from Equation 5.

The flow-occupancy plots for the advance detectors shown in Figure 20 clearly indicate the presence of the three traffic regimes in Figure 15. The plots from the two advance detectors were very similar, and thus only one of them is given. The calculated critical occupancies $\mathrm{Occ}_1^{\mathrm{adv}}$

and $\mathrm{Occ}_2^{\mathrm{adv}}$ are marked on the plots. These values are given in Table 6. They can be seen to match the transitions in the simulation graphs very closely.

The single occupancy threshold for stopline detectors was calculated for different simulations. These are shown on the flow-occupancy plots in Figure 21. As can be seen, the calculated values for the occupancy threshold match very closely with the transition in the simulated flow-occupancy plots.

Note also that the diagrams reflect the traffic states that were created in the simulation. For example, the first few hours in the simulation had a relatively low demand, corresponding to uncongested traffic. It can be seen on the graphs in Figure 20 and Figure 21 that points from 12 AM -6 AM are all below either $\mathrm{Occ}_1^{\mathrm{adv}}$ or $\mathrm{Occ}_{\mathrm{stp}}$. In addition, queue spillback was not introduced by the signal settings until 5 PM. Figure 20 and Figure 21 also show that the points in the queue spillback regime (above either $\mathrm{Occ}_2^{\mathrm{adv}}$ or $\mathrm{Occ}_{\mathrm{stp}}$) are all from 5 PM or later.

From these results, we have confirmed that: (i) AIMSUN can generate traffic patterns consistent with field observations; and (ii) the derived occupancy thresholds are valid since they match field observations and simulation results very well.

Table 6 Calculated values for occupancy thresholds under different simulated scenarios.

	Advance		Stopbar
Green time of Intersection 1	Occ_1^{adv}	Occ_2^{adv}	Occ_{stp}
25s	6.26 %	78.49 %	86.81 %
20s	5.01 %	82.79 %	89.44 %
15s	3.76 %	87.09 %	92.08 %
10s	2.51 %	91.39 %	94.72 %

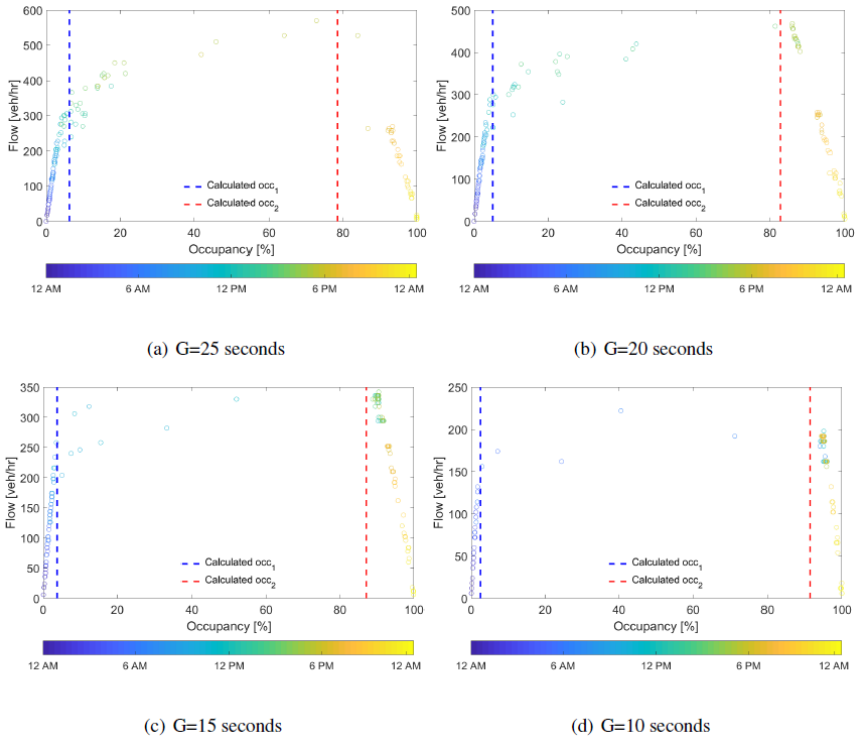

(a) G=25 seconds (b) G=20 seconds

(c) G=15 seconds (d) G=10 seconds

Figure 20 Flow-occupancy plots of advance detectors from simulations with various green times.

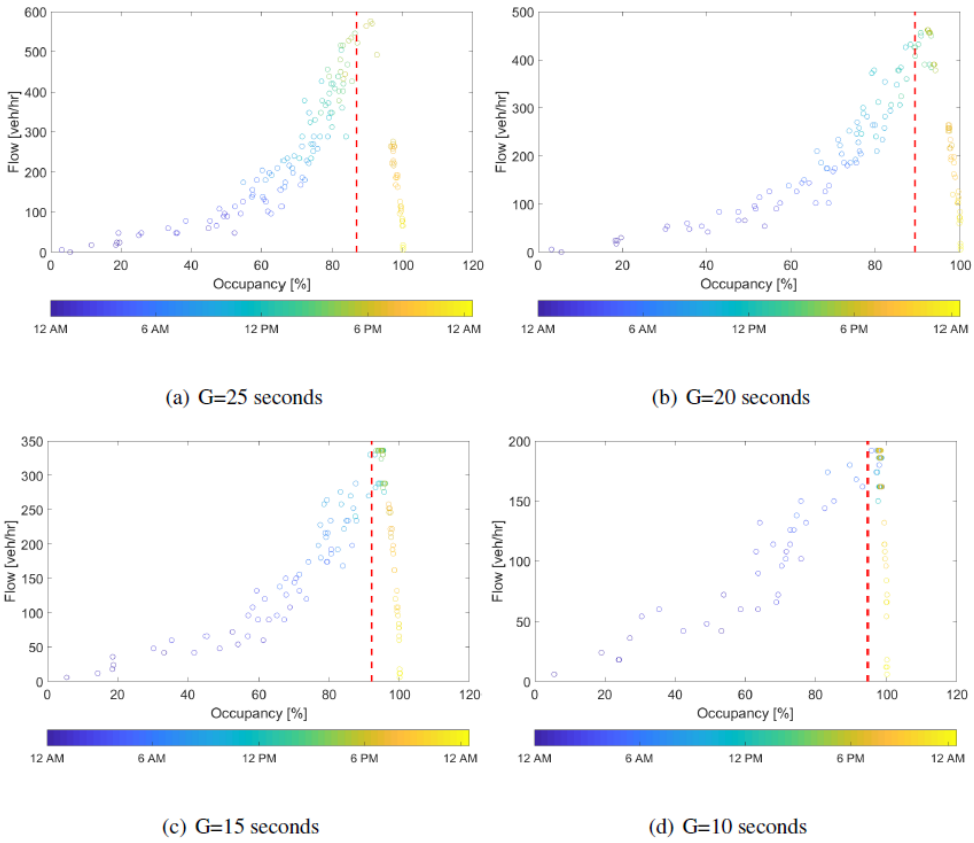

(a) G=25 seconds (b) G=20 seconds

(c) G=15 seconds (d) G=10 seconds

Figure 21 Flow-occupancy plots of stopline detectors from simulations with various green times.

3.3 Development of Estimation Algorithm

In this section, we are interested in estimating traffic states and queues at an intersection approach with given inputs of road geometry, detector layout, and identified traffic states at advance and stopline detectors.

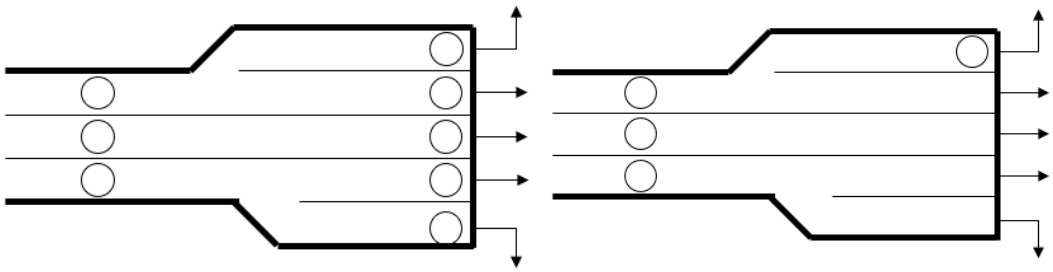

(a) Complete detector coverage (b) Partially complete detector coverage

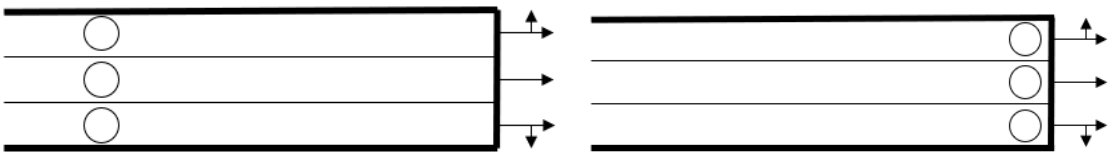

(c) With only advance detectors (d) With only stopline detectors

Figure 22 Four major types of sensor placement in the field.

3.3.1 Examples of Detector Layout at an Intersection Approach

At an intersection approach, it normally consists of three types of traffic movements: left-turn, straight through, and right-turn. Depending on the road geometry and the type of traffic control, we normally can see four major types of detector layout in the field, which is provided in Figure 22. Detailed descriptions are provided below:

(i) Complete detector coverage

As shown in Figure 22(a), both advance and stopline detectors are installed at a given intersection approach. It is clear to see that: (a) advance detectors detect all traffic movements, and (b) for each traffic movement, at least one stopline detector is allocated. Therefore, we consider this as complete detector coverage since we can tell traffic states for each movement by using the data from both advance and stopline detectors.

(ii) Partially complete detector coverage

In Figure 22(b), advance detectors are installed to detect all traffic movements. However, there is only one stopline detector installed for the left-turn movement, and none for the through and right-turn movements. Therefore, detector coverage is complete for the left-turn movement, but is incomplete for the other two movements. In this case, we consider this detector layout as partially complete.

(iii) With only advance detectors

In Figure 22(c), only advance detectors are installed to detect all traffic movements. This detector layout often occurs in minor streets. In this case, we can only tell traffic states in the upstream (in the vicinity of advance detectors), not in the downstream (in the vicinity of stopline). Therefore, this detector layout is incomplete.

(iv) With only stopline detectors

In Figure 22(d), only stopline detectors are installed to detector all traffic movements. This detector layout also often occurs in minor streets. In this case, we can only tell traffic states in the downstream (in the vicinity of stopline detectors), not in the upstream. Therefore, we consider this detector layout is incomplete. In addition, given the fact that we only can apply the second occupancy threshold to stopline detectors, we tell less traffic states solely based on stopline detectors.

3.3.2 Detector Groups for Different Traffic Movements

In the field, advance detectors are installed to detect one or more traffic movements. Based on our observations, we can have the following types of advance detectors:

(i) Advance for all movements
(ii) Advance for left turn only
(iii) Advance for right turn only
(iv) Advance for through only
(v) Advance for left turn and through
(vi) Advance for left turn and right turn
(vii) Advance for through and right turns

Similarly, we can have the following types of stopline detectors:

(i) Stobline for all movements
(ii) Stopline for left turn only
(iii) Stopline for right turn only
(iv) Stopline for through only
(v) Stopline for left turn and through
(vi) Stopline for left turn and right turn
(vii) Stopline for through and right turn

For the aforementioned detector types, the compositions (proportions) of traffic movements are different, which are location dependent and changing over time. In our study, we have default proportions of traffic movements at these detectors, which are provided in Table 7. However, we also update these values if we have complete detector coverage and good data is available.

Therefore, for the left-turn, through, and right-turn movements, we can have different detector groups:

(i) Left-turn

a. *Advance detector group*: Advance for all movements, Advance for left turn only, Advance for left turn and through, and Advance for left turn and right turn.
b. *Stopline detector group*: Stopline for all movements, Stopline for left turn only, Stopline for left turn and through, and Stopline for left turn and right turn.

(ii) Through

a. *Advance detector group*: Advance for all movements, Advance for through only, Advance for left turn and through, Advance for through and right turn.
b. *Stopline detector group*: Stopline for all movements, Stopline for through only, Stopline for left turn and through, Stopline for through and right turn.

(iii) Right-turn

a. *Advance detector group*: Advance for all movements, Advance for right turn only, Advance for left turn and right turn, Advance for through and right turn.

b. *Stopline detector group*: Stopline for all movements, Stopline for right turn only, Stopline for left turn and right turn, Stopline for through and right turn.

Table 7 Default proportions of traffic movements at advance and stopline detectors.

Detector Type	Default Proportions		
	Left Turn	Through	Right Turn
Advance for all movement	0.15	0.8	0.05
Advance for left turn only	1.0	0	0
Advance for right turn only	0	0	1.0
Advance for through only	0	1.0	0
Advance for left turn and through	0.3	0.7	0
Advance for left turn and right turn	0.5	0	0.5
Advance for through and right turn	0	0.85	0.15
Stopline for all movement	0.15	0.8	0.05
Stopline for left turn only	1.0	0	0
Stopline for right turn only	0	0	1.0
Stopline for through only	0	1.0	0
Stopline for left turn and through	0.3	0.7	0
Stopline for left turn and right turn	0.5	0	0.5
Stopline for through and right turn	0	0.85	0.15

3.3.3 Aggregation of Detector States for a Given Traffic Movement

For a given advance detector, its traffic state can be categorized into three regimes: Uncongested, Congested and Queue Spillback. Considering data missing due to detector failure, we can assign four different index values to these states:

(i) 0 for No Data,

(ii) 1 for Uncongested,

(iii) 2 for Congested

(iv) 3 for Queue Spillback.

Similarly, for a given stopline detector, we assign three different index values to the following states:

(i) 0 for No Data,

(ii) 1 for Uncongested

(iii) 2 for Congested/Queue Spillback

In the field, it is possible to have multiple detectors allocated to detect the same traffic movement, for example, the through movement in Figure 23. In the upstream, three advance detectors are assigned: A1 for left turn and through, A2 for through only, and A3 for through and right turn. Also, in the downstream, three stopline detectors are assigned: S2 for left turn and through, S3 and S4 for through only.

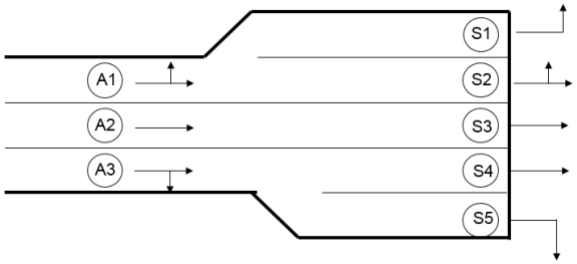

Figure 23 Example of traffic state aggregation at a given approach

In the upstream, all detectors, i.e., A1, A2 and A3, will provide their estimates of traffic states. Therefore, it is necessary to aggregate them from detector-level to movement-level (or approach-level). Normally, we can assign higher weights for detectors with exclusive movements, e.g., A2, and lower weights for detectors with shared movements, e.g., A1 and A3. In our case, we believe traffic is correlated between adjacent detectors sharing a common traffic movement. That means if traffic is congested at one detector, traffic at other detectors with a common traffic movement is expected to be congested. Therefore, we weight them according to the number of lanes they cover and the corresponding proportions of that common traffic movement.

For a given traffic movement, $m \in [LT, TH, RT]$, consider there are J advance detectors involved. Then the index of advance detectors for that traffic movement can be simply calculated as

$$\boldsymbol{Idx_{adv}^{m}} = \frac{\sum_{j \in J} \boldsymbol{Idx_{adv,j} \times n_{adv,j} \times prop_{adv,j}^{m}}}{\sum_{j \in J} \boldsymbol{n_{adv,j} \times prop_{adv,j}^{m}}}, \quad \textbf{(11)}$$

where $n_{adv,j}$ is the number of lanes advance detector j covers, and $\mathrm{prop}_{\mathrm{adv,j}}^{\mathrm{m}}$ is the proportion of movement m at advance detector j.

Similarly, suppose there are S stopline detectors involving the same traffic movement, $m \in [LT, TH, RT]$. The index of stopline detectors for that traffic movement can be simply calculated as

$$\boldsymbol{Idx_{stp}^{m}} = \frac{\sum_{s \in S} \boldsymbol{Idx_{stp,s} \times n_{stp,s} \times prop_{stp,s}^{m}}}{\sum_{s \in S} \boldsymbol{n_{stp,s} \times prop_{stp,s}^{m}}}, \quad \textbf{(12)}$$

where $n_{\mathrm{stp,s}}$ is the number of lanes stopline detector s covers, and $\mathrm{prop}_{\mathrm{stp,s}}^{\mathrm{m}}$ is the proportion of movement m at stopline detector s.

3.3.4 State Determination for a Given Traffic Movement

Once we calculate the indexes of advance and stopline detectors, i.e., Idx_{adv}^{m} and Idx_{stp}^{m}, we can use different thresholds that partition the state space into multiple regimes.

For stopline detectors, we have one threshold $Threshold_{stp}$ with a value of 1.5, which is the averaged index value of Uncongested (value=1) and Congested/Queue Spillback (value=2). Similarly, for advance detectors, we have two thresholds:

(i) $Threshold_{adv}^{low}$ =1.5, which is the averaged index value of Uncongested (value=1) and Congested (value=2),

(ii) $Threshold_{adv}^{high} = 2.5$, which is the averaged index value of Congested (value=2) and Queue Spillback (value=3).

Note that, these thresholds are set empirically, which can be fine turned in the future to obtain better results.

In the following, we will provide detailed discussion on how to partition the state space under different cases of detector coverage.

3.3.4.1 With Full Coverage of Advance and Stopline Detectors

For a given traffic movement, if both advance and stopline detectors exist, its state space can be categorized into six different regimes, which is shown in Figure 24. Details are provided below:

(i) **R1 ($Idx_{adv}^{m} \leq Threshold_{adv}^{low}$ and $Idx_{stp}^{m} \leq Threshold_{stp}$): No Congestion**

When both stopline and advance detectors report "Uncongested", it is clear that there is no congestion for the given traffic movement. Therefore, traffic states in this regime are categorized as "No Congestion".

(ii) **R2 ($Threshold_{adv}^{low} < Idx_{adv}^{m} \leq Threshold_{adv}^{high}$ and $Idx_{stp}^{m} \leq Threshold_{stp}$): Congestion With Downstream Free**

It is possible that stopline detectors report "Uncongested" while advance detectors report "Congested". This case may be caused by: (a) high upstream arrival rates but bad signal coordination; (b) unknown interruptions by other traffic movements within the area between the stopline and the advance detectors. In such a case, traffic states in this regime are categorized as "Congestion With Downstream Free".

(iii) **R3 ($Threshold_{adv}^{high} < Idx_{adv}^{m}$ and $Idx_{stp}^{m} \leq Threshold_{stp}$): Lane Blockage By Other Movements**

When queue spillback is found at advance detectors but stopline detectors indicate traffic is uncongested, it is possible this traffic movement is blocked by other movements. For example, through vehicles are often blocked by left-turn ones if the allocated green time is not able to clear the left-turn vehicles arriving from the upstream. In such a case, the stopline detectors that detect through vehicles will

report low occupancies, while the advance detectors will report high occupancies. Therefore, traffic states in this regime are categorized as "Lane Blockage By Other movements".

(iv) **R4 ($Idx_{adv}^{m} \leq Threshold_{adv}^{low}$ and $Idx_{stp}^{m} > Threshold_{stp}$): Light Congestion Caused By Downstream Traffic**

It is possible that downstream traffic is congested, either caused by temporary queue spillback or cycle failures. In this case, stopline detectors will report "Congested/Queue Spillback". However, advance detectors will report "Uncongested" since the downstream congestion is temporary and short queues exist at the given approach. Therefore, traffic states in this regime are categorized as "Light Congestion Caused By Downstream Traffic".

(v) **R5 ($Threshold_{adv}^{low} < Idx_{adv}^{m} \leq Threshold_{adv}^{high}$ and $Idx_{stp}^{m} > Threshold_{stp}$): Heavy Congestion Caused By Downstream Traffic**

If the downstream congestion lasts for a sufficient long time, the residual queue at the given approach may grow longer and interrupt vehicle passages at the advance detectors. In this case, stopline detectors will report "Congested/Queue Spillback", while advance detectors will report "Congested". Therefore, traffic states in this regime are categorized as "Heavy Congestion Caused By Downstream Traffic".

(vi) **R6 ($Threshold_{adv}^{high} < Idx_{adv}^{m}$ and $Idx_{stp}^{m} > Threshold_{stp}$): Queue Spillback Caused By Downstream Traffic**

A worse case is that the downstream congestion is heavy and lasts for a long time. As a result, a long queue is formed and spills back to the advance detectors. Then stopline detectors will report "Congested/Queue Spillback", while advance detectors will report "Queue Spillback". Therefore, traffic states in this regime are categorized as "Queue Spillback Caused By Downstream Traffic".

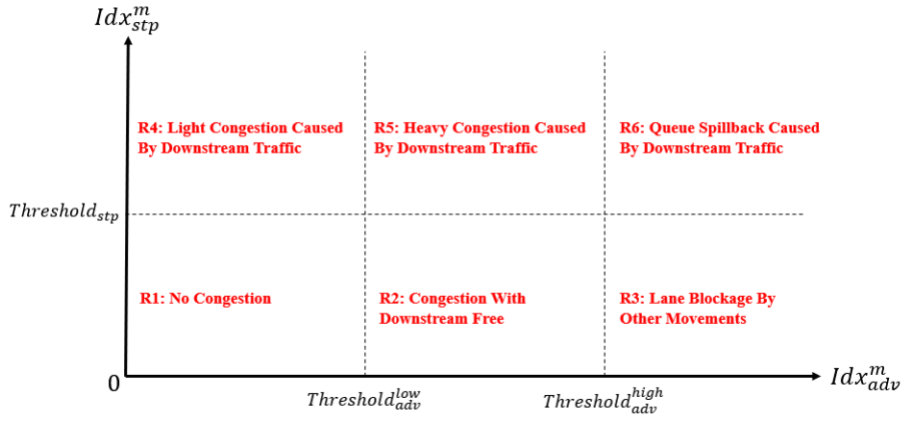

Figure 24 Traffic states for a given movement with full detector coverage.

3.3.4.2 With only Stopline Detectors Available

For some intersection approaches, particularly minor streets, it is possible to have only stopline detectors installed. In this case, we only can divide the state space into two regimes, which are shown in Figure 25. Details are provided below.

(i) **R1 ($Idx_{stp}^{m} \leq Threshold_{stp}$): No Congestion In Downstream**

When stopline detectors report "Uncongested", it is for sure the downstream traffic is free. However, traffic is free in the downstream may be due to: (a) relatively low upstream demands; or (b) lane blockages by other movements which restricts vehicles arriving from the upstream. Therefore, traffic states in this regime are categorized as "No Congestion In Downstream".

(ii) **R2 ($Idx_{stp}^{m} > Threshold_{stp}$): Downstream Congestion/Spillback**

When stopline detectors report "Congested/Queue Spillback", it is clear that the downstream traffic is congested, either caused by queue spillback from further downstream or inappropriate signal settings. However, without advance detectors, we don't know its impact on the arriving vehicles. Therefore, traffic states in this regime are categorized as "Downstream Congestion/Spillback".

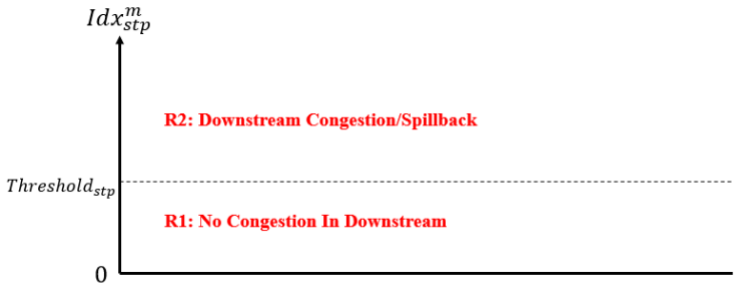

Figure 25 Traffic states for a given movement with only stopline detectors

3.3.4.3 With only advance detector available

It is normal to see only advance detectors are installed at the intersection approaches, particularly for minor streets. In this case, we can divide the state space into three different regimes, which are shown in Figure 26. Details are provided below:

(i) **R1 ($Idx_{adv}^{m} \leq Threshold_{adv}^{low}$): No Congestion In Upstream**

When advance detectors report "Uncongested", it only means upstream traffic is free. However, traffic in the downstream may be: uncongested or congested with a short queue. Therefore, traffic states in this regime are categorized as "No Congestion In Upstream".

(ii) **R2 ($Threshold_{adv}^{low} < Idx_{adv}^{m} \leq Threshold_{adv}^{high}$): Congestion In Upstream**

When advance detectors report "Congested", traffic is congested in the upstream (in the vicinity of advance detectors). It is probably caused by: (a) downstream congestion with a relatively long queue that interrupts vehicle arrivals from the

upstream; or (b) lane blockage by other traffic movements that reduces vehicle's throughput. Therefore, traffic states in this regime are categorized as "Congestion In Upstream".

(iii) R3 ($Threshold_{adv}^{high} < Idx_{adv}^{m}$): Queue Spillback In Upstream

When advance detectors report "Queue Spillback", a long queue should be formed that reaches the location of advance detectors. But in the downstream, it is not clear whether traffic is also congested or lane blockage occurs. Therefore, traffic states in this regime are categorized as "Queue Spillback In Upstream".

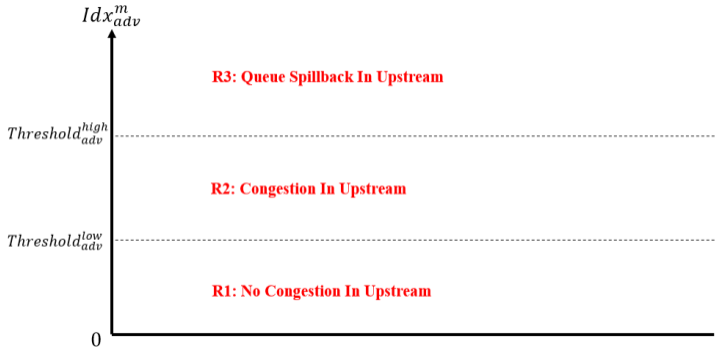

Figure 26 Traffic states for a given movement with only advance detectors

3.3.5 Queue Estimation of Traffic Movements at an Intersection Approach

In this subsection, given the estimated traffic state for a traffic movement, we are going to estimate an appropriate queue length, i.e., number of queued vehicles. Note that these queue estimates are in the "averaged" sense since the data we have is aggregated into a long time interval, e.g., 5 minutes.

3.3.5.1 Three Different Queue Thresholds

As shown in Figure 27, we first calculate three different queue thresholds for each traffic movement, which will be used as inputs to determine the queue length. Suppose there are N_{down} lanes in the downstream, and N_{up}lanes in the upstream. Note that N_{up} is not necessarily the same as N_{down} if there are turning pockets in the downstream. For lane i, the composition of each movement, $m \in [LT, TH, RT]$, is denoted as $prop_i^m$. The jam spacing for a regular automobile is denoted as L_{jam}. The length of lane i is denoted as L_i, and the distance to advance detectors is denoted as L_{adv}.

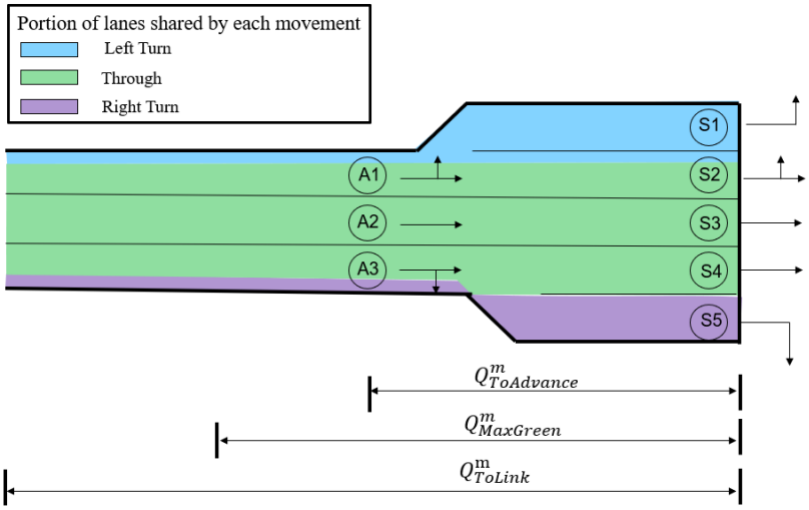

Figure 27 Three proposed queue thresholds for a given traffic movement.

In developing these thresholds, we consider: (a) different queue thresholds represent different levels of traffic congestion; (b) different lanes have different compositions of traffic movements; (c) the blockage of a certain movement cannot totally block other movements. Details are provided below:

(i) Queue To Advance Detector, $Q^m_{ToAdvance}$.

When traffic is uncongested, depending on the arrival time of vehicle platoons, a short queue may exist at the stopline and even temporarily spill back to the location of advance detectors. However, the allocated green time is long enough to clear the upstream arrival flow. As a result, there is no residual queue exists at the end of each green time.

While averaging the queue dynamics, we introduce $Q^m_{ToAdvance}$ to consider the boundary case when the averaged queue of movement m reaches the advance detectors. The calculation of $Q^m_{ToAdvance}$ can be formulated as

$$Q^m_{ToAdvance} = \frac{\sum_{i=1}^{N_{down}} min\{L_{adv}, L_i\} \times prop_i^m}{L_{jam}} \quad (13)$$

Note if there is detector coverage on lane i, $prop_i^m$ can be updated using the detector data from the field.

(ii) Queue With Max Green, $Q^m_{MaxGreen}$.

When the upstream arrival flow reaches the capacity that the allocated green time can handle, a residual queue will appear after the end of green time in each cycle. If the upstream arrival flow is temporarily over the capacity, the residual queue can grow and spill back to the advance detectors. When the residual queue reaches the location of advance detectors, the advance detectors can only detect a single constant

occupancy no matter how many vehicles arriving from the upstream, which is Point B in Figure 1. This residual queue may be so long that it spills back to the upstream intersection.

Therefore, we introduce another threshold $Q^m_{MaxGreen}$, which considers the case when the allocated green time is fully used and a residual queue reaches the advance detectors. The calculation of $Q^m_{MaxGreen}$ can be formulated as

$$\boldsymbol{Q^m_{MaxGreen} = Q^m_{ToAdvance} + \sum_{i=1}^{N_{down}} prop_i^m \times \frac{G}{h_s}} \quad \textbf{(14)}$$

Note $\sum_{\mathrm{i=1}}^{\mathrm{N_{down}}} \mathrm{prop_i^m}$ indicates the portion of lanes shared by the traffic movement m.

(iii) Queue To Link, Q^m_{ToLink}.

When the downstream traffic is congested, queue spillback will occur and partially block the vehicle dissipation at the targeted intersection. As a result, a vehicle has to wait for a longer time to cross the intersection, and the corresponding occupancy increases while the flow decreases. Meanwhile, a long queue will generate and propagate to the upstream.

Therefore, we introduce one more threshold Q^m_{ToLink} that consider the extreme case when movement m is totally blocked due to the queue spillback from the downstream. The calculation of Q^m_{ToLink} can be formulated as

$$\boldsymbol{Q^m_{ToLink} = Q^m_{ToAdvance} + \frac{\sum_{i=1}^{N_{up}} (L_i - L_{adv}) \times prop_i^m}{L_{jam}}} \quad \textbf{(15)}$$

3.3.5.2 With full coverage of advance and stopline detectors

When we have full coverage of advance and stopline detectors for a given traffic movement, traffic can be categorized into six different states. For each state, we have different calculations of queue lengths, which are determined through its average occupancy Occ from advance detectors and the three queue thresholds. Details are provided below and also in Figure 28.

(i) **R1**. In this regime, traffic is uncongested. Therefore, we only assign a small number of queued vehicles for the given traffic movement.

$$\boldsymbol{Q = Q^m_{ToAdvance} \times \frac{Occ}{Occ_1^{adv}}.} \quad \textbf{(16)}$$

(ii) **R2**. In this regime, traffic is congested, but the downstream is free. The allocated green time is long enough to clear the upstream arrivals, but not all of them (queued and arriving vehicles). Therefore, after each green time, a residual queue remains there. In this case, the number of queued vehicles is assigned between $Q^m_{ToAdvance}$ and $Q^m_{MaxGreen}$, depending on its average occupancy from advance detectors.

$$\boldsymbol{Q = Q^m_{ToAdvance} + \frac{Occ - Occ_1^{adv}}{Occ_2^{adv} - Occ_1^{adv}} (Q^m_{MaxGreen} - Q^m_{ToAdvance}).} \quad \textbf{(17)}$$

(iii) **R3**. In this regime, traffic is categorized as "Lane Blockage By Other Movements". Therefore, we expect a long queue. However, we will not assign any queued vehicles between the stopline and the advance detectors (the point where lane blockage is detected).

$$\boldsymbol{Q = (Q^{m}_{MaxGreen} - Q^{m}_{ToAdvance}) + (Q^{m}_{ToLink} - Q^{m}_{MaxGreen}) \frac{Occ - Occ_2^{adv}}{1 - Occ_2^{adv}}.} \quad \textbf{(18)}$$

(iv) **R4**. In this regime, traffic is a little bit congested, which is caused by downstream traffic. However, since the average occupancy from advance detectors is still low, we will use the same calculation in R1 for queue assignment.

(v) **R5**. In this regime, traffic is congested both in the upstream and the downstream. Therefore, we will use the calculation in R5 for queue assignment.

(vi) **R6**. In this regime, traffic is categorized as "Queue Spillback Caused By Downstream Traffic". In this case, no lane blockage occurs, and we will assign a long queue to the given traffic movement.

$$\boldsymbol{Q = Q^{m}_{MaxGreen} + (Q^{m}_{ToLink} - Q^{m}_{MaxGreen}) \frac{Occ - Occ_2^{adv}}{1 - Occ_2^{adv}}.} \quad \textbf{(19)}$$

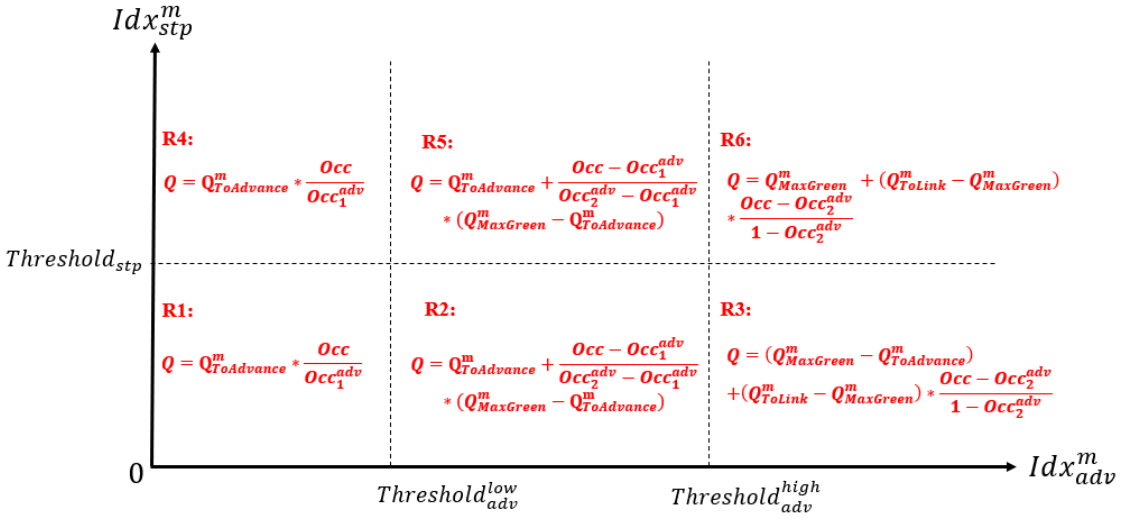

Figure 28 Calculation of vehicle queues with full detector coverage.

3.3.5.3 With only stopline detectors available

When we only have stopline detectors available, traffic can be categorized into two different states. Since only Occ_{stp} can be used, we have the following calculations for queue assignment, which is also provided in Figure 29.

(i) **R1**. In this regime, traffic is considered to be uncongested. Due to the impact of signal control, even a low vehicle arrival flow may cause high occupancies. Therefore, we only assign a short queue to the given traffic movement.

$$\boldsymbol{Q = (Q^{m}_{MaxGreen} - Q^{m}_{ToAdvance}) \frac{Occ}{Occ_{stp}}.} \quad \textbf{(20)}$$

Note this calculation is different from Equation 17, and Occ is the occupancy from the stopline detectors. Due to the impact of traffic signal, the maximum number we will assign is the maximum number of vehicles that can be released from the intersection approach, i.e., $\mathrm{Q}^{\mathrm{m}}_{\mathrm{MaxGreen}} - \mathrm{Q}^{\mathrm{m}}_{\mathrm{ToAdvance}}$.

(ii) **R2**. In this regime, traffic is congested, which may be caused by downstream spillback. In this case, we will assign a long queue to the given traffic movement.

$$\boldsymbol{Q = (Q^{m}_{MaxGreen} - Q^{m}_{ToAdvance}) + (Q^{m}_{ToLink} - Q^{m}_{MaxGreen} + Q^{m}_{ToAdvance}) \frac{Occ - Occ_{stp}}{1 - Occ_{stp}}} \quad \textbf{(21)}$$

Figure 29 Calculation of vehicle queues with only stopline detectors.

3.3.5.4 With only advance detectors available

In the case when only advance detectors are available, traffic can be categorized into three different regimes. Detailed calculations are provided below as well as in Figure 30.

(i) **R1**. In this regime, traffic is uncongested in the upstream. Therefore, we use the calculation in R1 (or R4) in Figure 28.

(ii) **R2**. In this regime, congestion occurs in the upstream. However, there is no way to check whether downstream traffic is congested or not. Therefore, we use the calculation in R2 (or R5) in Figure 28.

(iii) **R3**. In this regime, queue spillback occurs in the upstream. Due to the lack of downstream detection, we are not able to further find out whether the congestion is caused by lane blockage or downstream queue spillback. Therefore, we use the calculation in R6 in Figure 28.

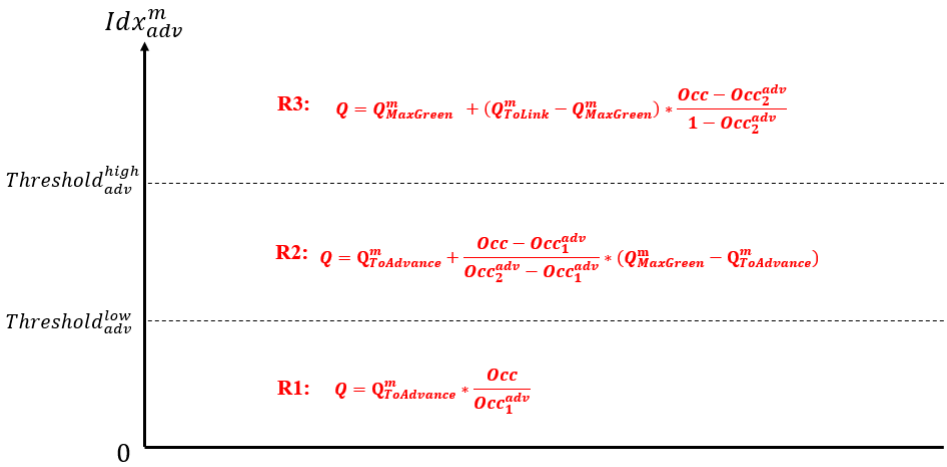

Figure 30 Calculation of vehicle queues with only advance detectors.

3.4 Validation

In this section, we are interested in assessing the queue estimation method proposed in Section 3.3. In particular, we would like to validate whether the queue estimates are consistent with real-world observations. In practice, it is very difficult and time consuming to validate against with the actual queues in a test site. Therefore, we would like to validate the relation between vehicle queues and some conventional, easy-to-access measurements, e.g., Bluetooth travel times. Details are provided in the following subsections.

3.4.1 A linear relation between vehicle queue and travel time

According to (Herman and Prigogine, 1979), traffic in urban networks can be categorized into two different traffic states: (i) queued at the intersection, and (ii) moving across a link with an average speed v_0. Therefore, the time for a vehicle to travel across a link consists of two parts: (i) queueing time t_{queue} at the intersection, and (ii) link travel time t_{move}.

To measure travel delay at a given intersection, a prevailing method is the one proposed by the Highway Capacity Manual (TRB, 2000). In the HCM calculation, the average delay d for a traffic movement consists of three different components: (i) uniform delay d_1, (ii) incremental delay d_2, and (iii) initial queue delay d_3. Detailed formulation is provided below.

$$\boldsymbol{d = d_1 + d_2 + d_3},$$

$$\boldsymbol{d_1 = \frac{0.5C\left(1-\frac{G}{C}\right)^2}{1-\frac{G}{C}min\{1,X\}}},$$

$$\boldsymbol{d_2 = 900T[(X-1) + \sqrt{(X-1)^2 + \frac{8kIX}{cT}}]},$$

$$\boldsymbol{d_3 = \frac{1800Q_b(1+\mu)\tau}{cT}},$$

$$\tau = \begin{cases} 0 & Q_b = 0 \\ min(T, \frac{Q_b}{c(1-min(1,X))}) & otherwise \end{cases}$$
$$\mu = \begin{cases} 0 & \tau < T \\ 1 - \frac{cT(1-min(1,X))}{Q_b} & otherwise \end{cases} \quad (22)$$

where c is the capacity, X is the ratio of flow rate to capacity (f/c), T is the analysis time period, I is the upstream filtering/metering adjustment factor, k is the incremental delay factor, and Q_b is the initial queue.

When traffic is congested, i.e., $X \geq 1$, the delay calculation can be rewritten as

$$d = \alpha\left(X, c, \frac{G}{C}\right) + \beta(c)Q_b, \quad (23)$$

where $\alpha(.)$ and $\beta(.)$ are functions. If signal settings (G/C) remain unchanged and arrival flow f changes slowly in the analysis time period T, the evolution of queue lengths for a given traffic movement follows the pattern in Figure 31. Therefore, the average queue Q_{avg} can be computed as

$$Q_{avg} \approx Q_b + \theta(X, c, \frac{G}{C}), \quad (24)$$

where $\theta(.)$ is also a function.

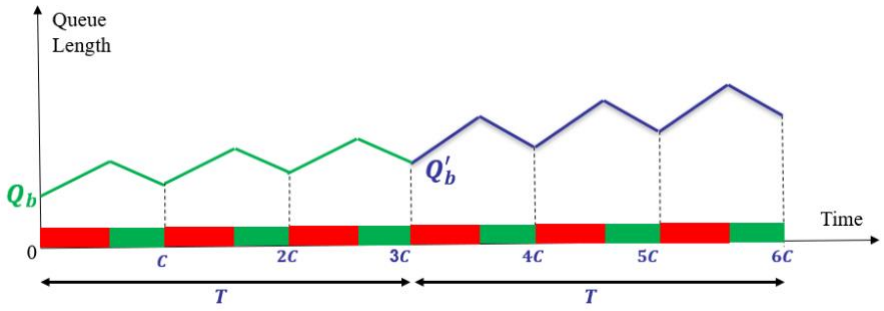

Figure 31 Evolution of queue lengths under near-stationary states for a given traffic movement.

Let's consider n intersections along a corridor, which have similar road geometries and signal settings. Also, we assume the demands of left-turn and right turn vehicles are low to ensure minimal interactions with the through vehicles. The total time tt for through vehicles crossing these intersections consists of the queueing time and the travel time with speed v_0, which can be computed as

$$\begin{aligned} tt &= \sum_{i=1}^{n}\left[\frac{L_i}{v_0} + \alpha_i\left(X_i, c_i, \frac{G_i}{C_i}\right) + \beta_i(c_i)Q_{b,i}\right] \\ &= \sum_{i=1}^{n}\frac{L_i}{v_0} + \sum_{i=1}^{n}\left[\alpha_i\left(X_i, c_i, \frac{G_i}{C_i}\right) + \beta_i(c_i)Q_{b,i}\right] \\ &\approx \sum_{i=1}^{n}\frac{L_i}{v_0} + \sum_{i=1}^{n}\left[\alpha_i\left(X_i, c_i, \frac{G_i}{C_i}\right) + \beta_i(c_i)\theta_i\left(X_i, c_i, \frac{G_i}{C_i}\right) + \beta_i(c_i)Q_{avg,i}\right] \end{aligned}$$

$$= \sum_{i=1}^{n} \frac{L_i}{v_0} + \sum_{i=1}^{n} \phi_i \left(X_i, c_i, \frac{G_i}{C_i}\right) + \sum_{i=1}^{n} \beta_i(c_i) Q_{avg,i}$$
$$\approx \frac{nL}{v_0} + n\phi \left(X, c, \frac{G}{C}\right) + \beta(c) \sum_{i=1}^{n} Q_{avg,i}$$
$$= \boldsymbol{tt_{v_0} + tt_{queue}} \left(\boldsymbol{X, c, \frac{G}{C}}\right) + \boldsymbol{\beta(c) Q_{tot}} \quad \textbf{(25)}$$

where $L_i \approx L$, $X_i \approx X$, $c_i \approx c$, $\frac{G_i}{C_i} \approx \frac{G}{C}$, $\phi_i(.) = \alpha_i \left(X_i, c_i, \frac{G_i}{C_i}\right) + \beta_i(c_i)\theta_i \left(X_i, c_i, \frac{G_i}{C_i}\right) \approx \phi(.)$, and $\beta_i \approx \beta$. In addition, we denote $tt_{v_0} = \frac{nL}{v_0}$, $tt_{queue} \left(X, c, \frac{G}{C}\right) = n\phi \left(X, c, \frac{G}{C}\right)$, and $Q_{tot} = \sum_{i=1}^{n} Q_{avg,i}$. Note that Q_{tot} is the total vehicle queues (in the averaged sense) of the through movement for a single direction along these n intersections.

From Equation 26, it is clear to see there exists a linear relation between the total travel time tt and the total vehicle queue Q_{tot} for the through movement. Furthermore, if the left-turn and right-turn demands are relatively low, traffic dynamics at a given intersection approach is dominated by the through vehicles. In such a case, we also expect this linear relation is valid between the total travel time and the total vehicle queues of all traffic movements. Therefore, we have the following conjecture.

Conjecture: ***Under congested traffic conditions, the total travel time crossing multiple intersections along a corridor is linearly related to the total vehicle queues at these intersection approaches when: (i) these intersections have similar road geometries and signal settings; and (ii) the left-turn and right-turn demands are relatively low.***

Note that one reason of having the above conjecture for all traffic movements instead of through movement only is because it is difficult to have consistent and accurate queue estimates for through vehicles due to incomplete detector layouts in the field.

In the following subsections, we are going to validate this linear relation using Bluetooth travel times from the field and the queue estimates from our proposed method.

3.4.2 Study Site and Data Sources

The selected study site consists of five intersections along Huntington Dr in the City of Arcadia, CA and is shown in Figure 32: @Santa Clara St, @ Santa Anita Ave, @First Ave, @Second Ave, and @Gateway Dr. Within the study site, we have good detector coverage, particularly along the eastbound and the westbound directions. In addition, we have two Bluetooth stations installed in this study site: one is at Huntington Dr & Santa Clara St, while the other is at Huntington Dr & Gateway Dr. As shown in the figure (partial information is also provided in Figure 6), these five intersections have similar road geometries in the eastbound and the westbound directions. Also, according to the timesheets from the field (partial information is also provided in Figure 7 and Table 2), these intersections have similar settings of traffic signals. Therefore, this is a good study site to validate the conjecture on the linear relation between the total travel time and the total (averaged) vehicle queue in the eastbound and the westbound directions.

Figure 32 Study site for validation

Here, the travel time data is retrieved from the Bluetooth stations. However, given the low penetration rates of vehicles equipped with Bluetooth devices, we collected the data for four months, from 2016-01-01 to 2016-04-30, and used the weekday travel time profile (median values) for validation.

Similarly, detector data and signal phasing data within the same period were collected from Arcadia's TCS servers. The detector data is aggregated into five minutes, while the signal phasing data is reported cycle by cycle. In addition, we can get the planned signal phasing settings from the timesheets in the field. All the above information is used as inputs into the queue estimation model proposed in previous sections.

3.4.3 Validation Results

Figure 33 illustrates the relation between the estimated total queues and the Bluetooth travel times in the eastbound direction. From the weekday profiles in Figure 33(a), we can find that traffic is congested in the afternoon peak period, from 2 PM to 8 PM. During this time periods, we do see a strong correlation between the estimated total queues and the Bluetooth travel times. Therefore, we performed a regression analysis on the data selected in this time period (i.e., in the red-dashed rectangle), and the results are provided in Figure 33(b). Clearly, a strong linear relation exists with a R-Square of 0.72.

Similarly, we extend our analysis to the westbound direction, and the results are provided in Figure 34. Clearly, from Figure 34(a), traffic is congested in the morning peak period, from 6AM to 10AM. We performed the same regression analysis on the data selected in this time period (i.e., in the red-dashed rectangle), and find a strong linear correlation with a R-Square of 0.72. The results are shown in Figure 34(b).

Based on the above analysis, it is confirmed that the conjecture on the linear relation between the estimated total queue and the observed travel time is valid. That also means the proposed queue estimation is valid and can produce reasonable estimates consistent with real-world observations.

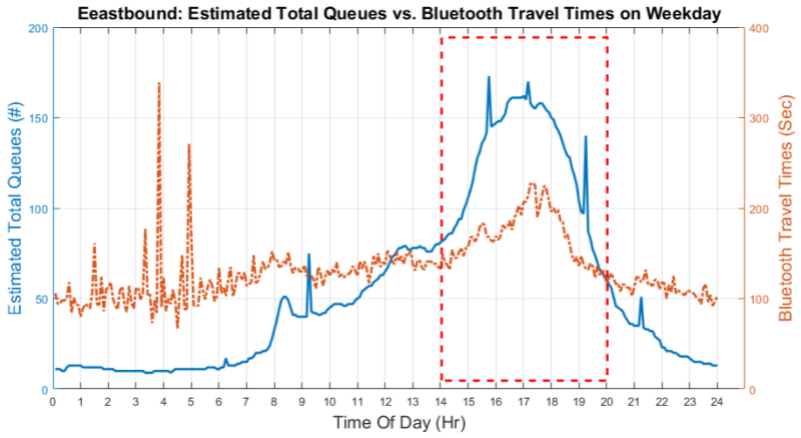

a. Weekday profiles

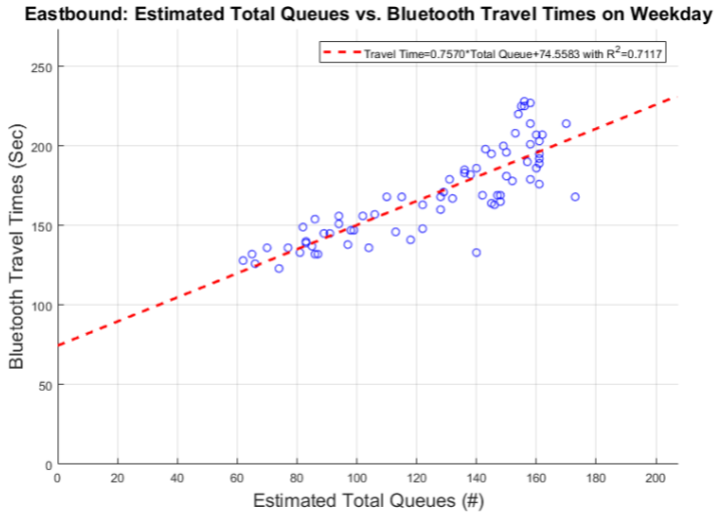

(b) Linear relation in the selected afternoon peak period

Figure 33 Relation between estimated total queues and Bluetooth travel times in the EB direction.

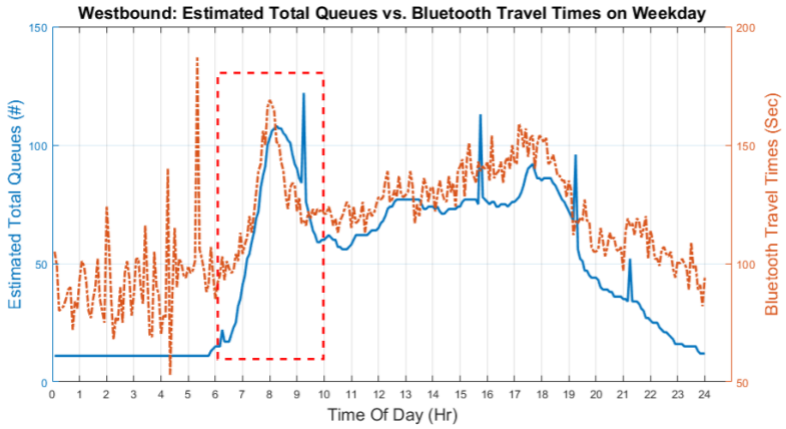

a. Weekday profiles

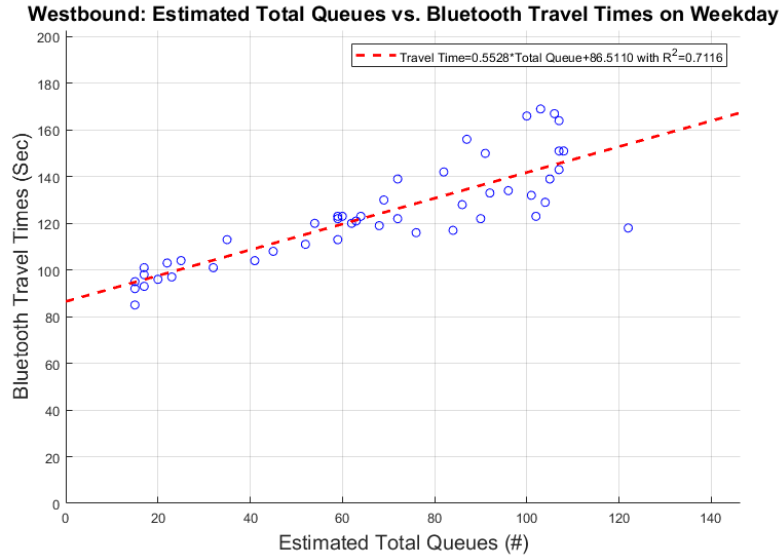

(b) Linear relation in the selected morning peak period

Figure 34 Relation between estimated total queues and Bluetooth travel times in the WB direction.

3.5 Traffic Initialization from Estimates of Traffic States and Queues

In Section 3.4, we have proposed methods to estimate traffic states and queues from detector and signal phasing data. In this section, we will introduce how to apply these estimates for the purpose of traffic initialization in microsimulations.

3.5.1 Framework of Traffic Estimation and Initialization in AIMSUN

In Figure 35, we provide the framework of traffic estimation and initialization in AIMSUN. It consists of the following components:

(i) Data Archive

The database is used to host multiple sources and types of data: (a) detector data and signal information from the field; and (b) network information and simulation data from the AIMSUN model. The data from field detectors contains flows and occupancies at the interval of five minutes, while the signal information contains both planned and actual cycle lengths and green times for the phases. The network from the AIMSUN model is an important input for both estimation and initialization, which contains detailed information of nodes, sections, and detectors. Considering the AIMSUN model is well calibrated, a set of simulation data is required for initialization. Particularly, OD information within a link is an important input for initialization since we need to assign a vehicle with a certain OD to tell where it should go. Other statistics such as lane-based speed and flow are also collected. In addition, it is normal to have intersections and links without detector coverage. Therefore, snapshots of vehicle trajectories are recorded in order to fill in appropriate number of vehicles inside these intersections and links.

(ii) Arterial Traffic Estimation.

For arterial traffic estimation, network information such as intersection geometries and detector locations and types is used as static inputs. Detector data and signal information, either real-time or historical, are used as dynamic inputs to assess the traffic states and queues for the available traffic movements at a given intersection approach. The estimation method follows the one proposed in Section 3.3. Due to the fact that detector data is aggregated into the interval of 5 minutes, the estimated states and queues are the "averaged" ones within 5 minutes.

(iii) Arterial Traffic Initialization.

In the initialization step, the output from the estimation step is used as one of the inputs. However, the estimated queues are the "averaged" ones within fixed time intervals. If one wants to initialize the network and kick off simulation at a certain time, it requires a method that can convert the average queue into different portions of moving and queued vehicles. Therefore, signal information is required to determine the signal state at a given time input. In order to place vehicles to a specific lane on a certain section, the AIMSUN network is required as input. Also, lane-based/link-based OD information is needed to tell a vehicle where it should go when we place it on a link. Other information such as speed is used to tell how fast a vehicle can travel within the link. In addition, considering not all intersections and links have detector coverage, we will use vehicles from AIMSUN simulations and place them on those links.

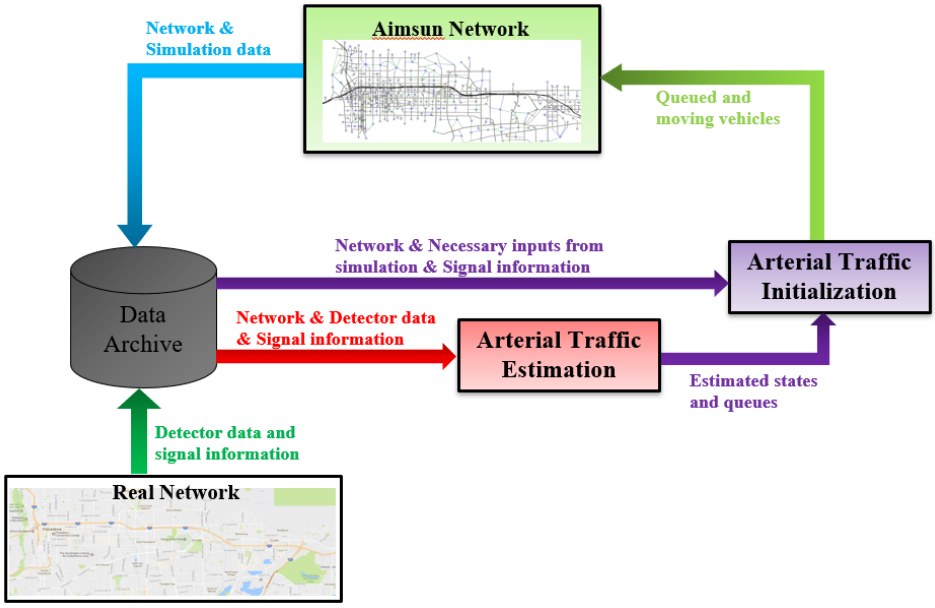

Figure 35 Framework of traffic estimation and initialization in AIMSUN.

3.5.2 Initialization Algorithms

At signalized intersections, there exist different compositions of vehicles during the green and red time periods. As shown in Figure 36, when the traffic light is red, there exist two portions of vehicles: one portion consists of queued vehicles that are waiting at the stopline for the next green period, while the other consists of moving vehicles from the upstream. However, when the traffic light turns green, there exist three portions of vehicles: one portion in the most downstream consists of vehicles moving with the saturation speed/headway; right after that, there may exist a portion that consists of queued vehicles which may be cleared before the end of green period; the third portion consists of moving vehicles that are generated from the upstream intersections.

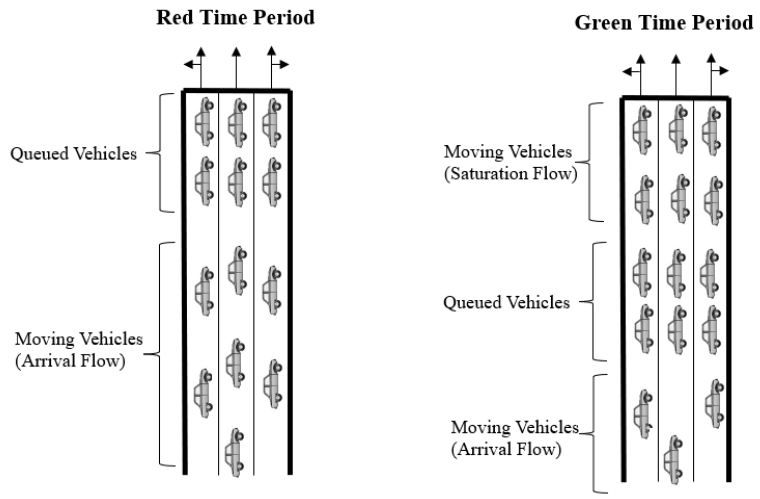

Figure 36 Composition of vehicles at a signalized intersection approach.

In our case, we want to simplify the compositions of vehicles at a give intersection approach to only consider two portions of vehicles: (i) queued vehicles at the most downstream, and (ii) moving vehicles in the upstream. This simplification will introduce errors during the green time period. However, this error is not critical if we can have a good estimate of the traffic state and put a reasonable number of vehicles inside the link. Also, once simulation starts, this error will become a minor issue after one or two cycles.

The way to assign vehicles to a given intersection approach using the estimates of traffic states and queues is described below.

Algorithm: Vehicle Assignment

FOR each intersection approach
  IF estimates of states and queues are available
    - Determine the number of moving and queued vehicles according to the signal settings.
    - Assign OD information to these moving and queued vehicles.
    - Place these vehicles at the intersection approach.
      - ✓ From the downstream to the upstream.
      - ✓ Queued vehicles first, and moving vehicles next.
      - ✓ If a dedicated lane is full, assign vehicles to its adjacent lanes.

  ELSE
    - No initialization is needed. Use the vehicles from Aimsun simulations.

  END IF
END FOR

Particularly, at a certain time t, we use signal settings in the field to determine its current state: whether it is in the green or red time period, and how long it has been green or red. Based on this information, we can determine the portions of queued and moving vehicles.

As a first step, we need to know the minimum and maximum queue lengths for a given traffic movement under its current green time settings. Suppose the allocated green time is G, and the

saturation headway is h. Then the maximum number of vehicles that can be cleared by the allocated green time within a cycle can be computed as

$$\boldsymbol{N_{max} = \frac{G}{h}} \quad \textbf{(26)}$$

Then there are two cases in calculating the minimum and maximum queues, which are provided in Figure 37.

(i) **With no initial queue** when $N_{max} \geq 2Q_{avg}$

In this case, the minimum queue Q_{min} is

$$\boldsymbol{Q_{min} = 0} \quad \textbf{(27)}$$

And the maximum queue Q_{max} is

$$\boldsymbol{Q_{max} = 2 \times Q_{avg}} \quad \textbf{(28)}$$

(ii) **With an initial queue** when $N_{max} < 2Q_{avg}$

In this case, the minimum queue Q_{min} is

$$\boldsymbol{Q_{min} = \frac{2Q_{avg} - N_{max}}{2}} \quad \textbf{(29)}$$

And the maximum queue Q_{max} is

$$\boldsymbol{Q_{max} = Q_{avg} + \frac{N_{max}}{2}} \quad \textbf{(30)}$$

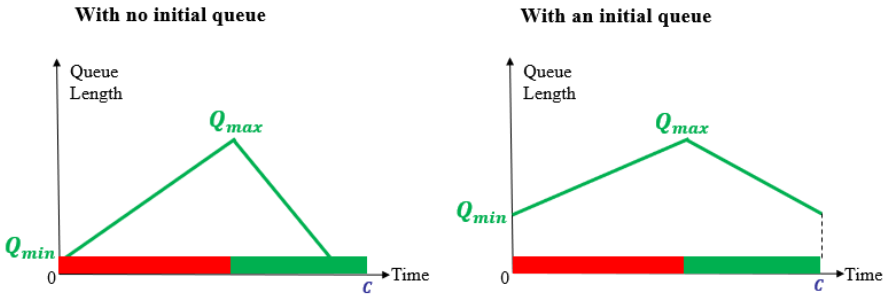

Figure 37 Estimation of minimum and maximum queue lengths with/without initial queues

After calculating the minimum and maximum queues, we consider:

(i) The number of vehicles within an arterial link (between two intersections) is Q_{max};

(ii) The portions of queued and moving vehicles are determined according to the current active traffic state (Geen/Red) and how long it has been in such a state.

Therefore, we can have the following calculations:

(i) Current signal state has been Green for $G_{act} \leq G$.

$$\boldsymbol{N_{move} = \frac{min\{G_{act}, hQ_{max}\}}{min\{hQ_{max}, G\}}(Q_{max} - Q_{min})} \quad \textbf{(31)}$$

$$N_{queue} = Q_{max} - N_{move} \quad (32)$$

(ii) Current signal state has been Red for $R_{act} \leq C - G$

$$\boldsymbol{N_{queue} = Q_{min} + \frac{R_{act}}{C-G}(Q_{max} - Q_{min})} \quad \textbf{(33)}$$

$$N_{move} = Q_{max} - N_{queue} \quad (34)$$

3.5.3 Application to the I-210 Connected Corridors Pilot

In this subsection, we illustrate how to apply this estimation-initialization framework to real networks, e.g., the I-210 Connected Corridors Pilot. Sensor placement (location & type) is provided in Figure 38(a), while the simulation network in AIMSUN is provided in Figure 38(b). Even though we have more than 400 intersections in this network, we now only have a stable data feed for the detectors in the City of Arcadia, which is highlighted with a red-dashed circle in Figure 38(a). Therefore, we only apply the estimation-initialization framework to the intersections with detector coverage in this city. For the rest of the network, including freeways and arterial road links, vehicles are generated from the simulation backup in AIMSUN. In the near future, when detector data is available for other cities, we will apply this framework to the whole corridor.

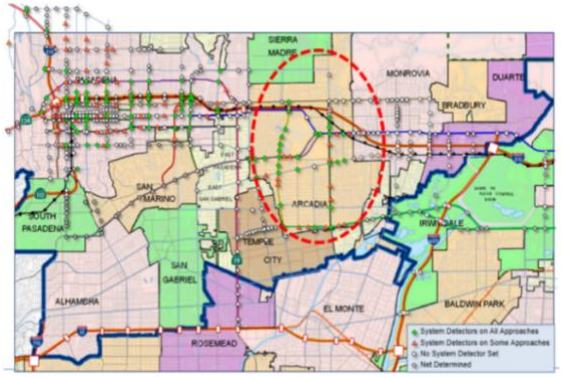

a. Sensor placement

(b) Simulation network in AIMSUN

Figure 38 Sensor placement and simulation network of the I-210 Connected Corridors Pilot.

Figure 39 demonstrates the traffic estimation-initialization framework in the study site (see Figure 6 and Figure 32) along Huntington Dr in Arcadia. For each intersection approach with detector coverage, queues are estimated using the proposed method in Section 3.3 and then are

converted into simulated vehicles using the initialization method in Section 3.5.2. As highlighted in Figure 39 (by red rectangle), these simulated vehicles are inserted into the designated links and lanes in the network using Python scripts: queued vehicles first, and moving vehicles next. For freeway links and intersections without detector coverage, vehicles are generated from the simulation backup and inserted back to the corresponding links and lanes in the network using Python scripts. An example is highlighted by the green-dashed rectangle in Figure 39.

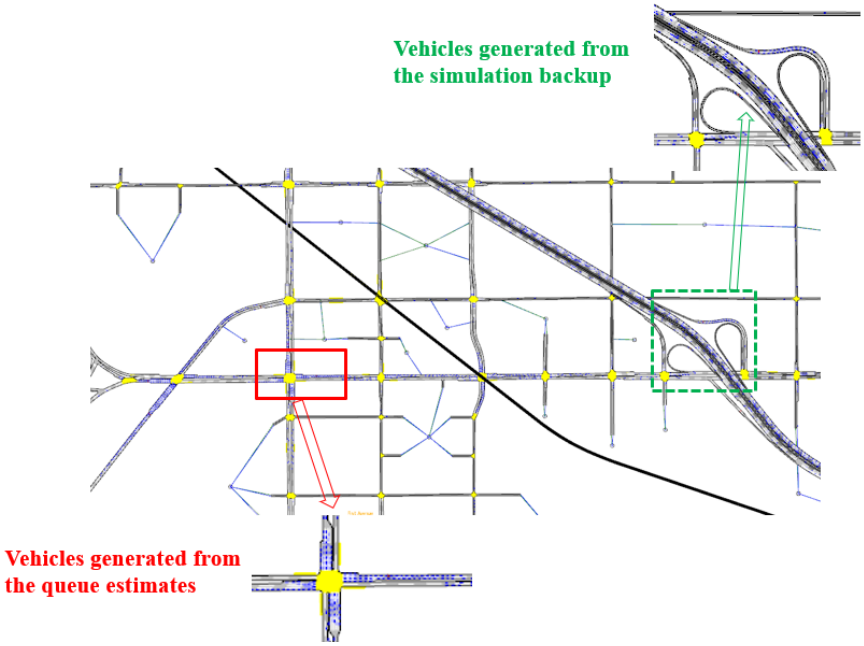

Figure 39 Demonstration of traffic estimation and initialization along Huntington Dr in Arcadia.

3.6 Discussion

In this part, we focused on the estimation of arterial traffic using the trapezoidal fundamental diagram proposed in Part II. We first demonstrated the validity of the two occupancy thresholds for advance and stopline detectors by showing a good fit with the data both from the field and microsimulations. Then we developed an estimation algorithm that handles various aspects in the field, such as incomplete detector layout and detection of mixed traffic movements. For each traffic movement, approach-level traffic states are assessed based on the estimated states from associated individual detectors, and average queues are determined based on these traffic states as well as the restrictions of road geometry and detector layout. Furthermore, we demonstrated the validity of the estimation algorithm by showing a strong correlation between the queue estimates and the observed Bluetooth travel times from the field. In addition, we developed an estimation-initialization framework to initialize traffic states in microsimulations in AIMSUN. The proposed initialization algorithm will generate simulated vehicles using the queue estimates and some other necessary inputs from the AIMSUN model. These simulated vehicles consist of two portions: queued vehicles and moving vehicles. They are inserted into the designated links and

lanes in the network using Python scripts accordingly: queued vehicles first and moving vehicles next. Such a framework was demonstrated using the I-210 AIMSUN model in the City of Arcadia. The proposed estimation-initialization framework is novel, which provides a fundamentally different way of state estimation and initialization. It is expected to outperform the conventional method given good detector coverage and data quality.

4. Part IV: Conclusion and Future Research

4.1 Conclusion

In this project, a novel approach has been developed to estimate traffic states on arterial road links using both loop detector data and signal phasing information. The approach consists of the following two tasks: (i) estimate the traffic flow fundamental diagrams for arterial road links that are used to categorize traffic states into different regimes; (ii) develop estimation algorithms that utilize the proposed fundamental diagram and produce estimates of traffic states and vehicle queues for the traffic movements at a given intersection approach.

The proposed arterial fundamental diagram is trapezoidal due to the presence of signal control. Two occupancy thresholds are proposed to divide traffic into three different regimes: uncongested, congested, and downstream queue spillback. The required parameters are closely related to road geometry, detector layout, and vehicle dynamics, and can be either retrieved or estimated from field data. In our development, we carefully analyzed the limitation of point detection as well as potential impacts of platoon dispersion, initial queue, and coordination level on the shape of the proposed trapezoidal fundamental diagram. We concluded that the proposed trapezoidal fundamental diagram is point-based and represents most of the traffic states at the link level. But it fails to detect more traffic states when traffic is extremely congested and the residual queue spills over the advance detectors. We also analytically and graphically demonstrated that the estimation of queue waiting time at advance detectors is accurate under minor platoon dispersion and the impact of initial queue can be ignored if we consider near-stationary traffic states. However, poor coordination level will significantly impact traffic performance, which drifts the observations in the flow-occupancy plots to the right with higher occupancies. By selecting a study site with three intersections along Huntington Drive in the City of Arcadia, we carefully analyzed the data from both advance and stopline detectors and decided to use the data from the former since the measurements are more reliable and less impacted by the traffic signal. In the proposed trapezoidal fundamental diagram, one of the key parameters is the saturation flow rate, which is lane specific and should be calibrated/estimated from field data. We proposed a calibration algorithm and applied it to estimate the saturation flow rates at the advance detectors in the study site. Results showed that the estimated saturation flow rate varies a lot, from 1200 veh/hr/ln to 2300 veh/hr/ln. We found that inappropriate detector placement, temporary lane blockage, slow turning movements, and active pedestrian crossings will significantly reduce the lane throughput, which as a result will lead to a low saturation flow rate. Furthermore, we developed an algorithm to estimate the upper bounds of the flow-occupancy plots, which is considered to represent the actual trapezoidal fundamental diagrams.

We then applied this algorithm to the advance detectors in the study site and compared the estimated upper bound with the estimated trapezoidal fundamental diagram. Results demonstrated that the estimated trapezoidal fundamental diagram generally matches the field data well with low MAPEs. Some exceptions with high MAPEs were found, which may be caused by: (i) the lack of enough data points, and (ii) poor coordination level.

Furthermore, we extended our study to estimate traffic states at intersection approaches based on the proposed trapezoidal fundamental diagram, particularly using the two occupancy thresholds. As a first step, we confirmed the validity of the two occupancy thresholds at both advance and stopline detectors since they matched both observed and simulated data very well. Then for a given intersection approach, we developed a novel estimation algorithm that takes into account different configurations of detector layouts and traffic movements. The estimated states and average queues for the traffic movements (left-turn, through, and right-turn) at an intersection approach are determined based on the traffic states at both advance and stopline detectors. When traffic is congested and no significant left-turn and right-turn movements at multiple intersections along an arterial corridor, we theoretically proved that there exists a linear relation between the total vehicle queues and the travel times. The relationship was validated on a segment of five intersections along Huntingtin Drive in the City of Arcadia using detector data and Bluetooth travel times. In addition, we developed a novel estimation and initialization framework that reads field data, estimates average vehicle queues, and generates simulated vehicles in the AIMSUN microsimulation software. We successfully applied such a framework to the arterial intersections in the City of Arcadia in the I-210 Connected Corridors pilot in AIMSUN.

4.2 Future Research Directions

As discussed above, efforts have been devoted to estimating the trapezoidal fundamental diagram and applying it to estimate traffic states on arterial road links. Such a comprehensive study provides building blocks for a number of future studies, which are listed below:

(i) Detection of lane blockage and queue spillback: Lane blockage and queue spillback often occur at arterial road intersections, particularly for left turns with insufficient green times. It may cause serious traffic problems if such a phenomenon occurs frequently and lasts for a long time. Luckily, the findings in our study provide a novel way to identify this phenomenon if the detector coverage is complete. As illustrated in previous chapters, we can apply the two occupancy thresholds to categorize traffic states into three regimes at advance detectors: Uncongested, Congested, and Downstream spillback. For stopline detectors, even though the flow-occupancy plots are messy, we demonstrated that it is still possible to apply the second occupancy threshold to categorize the traffic states into two regimes: Uncongested, Congested/Downstream spillback. Therefore, if one intersection approach has complete coverage of detectors, it is possible to identify potential lane blockages and downstream queue spillback using the estimated traffic states from both advance and stopline detectors. Such a detection can be real-time if the data stream is real-time. Also, we can develop a new performance metric to quantify the performance of signal

control at the intersection based on the occurring frequency of lane blockage and queue spillback.

(ii) Optimal traffic signal control: From our analysis, we can clearly see that the capacity of the trapezoidal fundamental diagram is closely related to the allocated green times to the traffic movements at the targeted intersection approach. A larger green ratio often results in a higher capacity. Meanwhile, coordination level plays another key role in traffic performance. A good coordination level will allow vehicles travel freely across the intersection without stopping, which as a result having a high flow rate with a low occupancy at both advance and stopline detectors.

For a given intersection approach, the inflow is actually the sum of outflows of upstream intersections. Therefore, the whole arterial network is connected since the control of one intersection is also related to the control of other intersections. In the future study, we are interested in developing adaptive signal control strategies for individual intersections based on the proposed trapezoidal fundamental diagram. The proposed control strategies aim to use the trapezoidal fundamental diagrams at the targeted intersection as the optimal references and try to adjust the green times and offset to minimize the total distances between the actual traffic flows and the optimal ones. The proposed control strategies are decentralized, which focuses on individual intersections. However, we would like to further investigate their system impacts on large-scale arterial networks.

(iii) Data fusion with probe trajectories: In this study, the proposed estimation algorithm purely relies on the data from loop detectors. However, several key aspects limit its applications. First of all, incomplete detector layout will reduce the estimation accuracy. In the field, for most of the cases, only left-turn movement has complete detector coverage with both advance and stopline detectors. For other traffic movements, e.g., through and right-turn, only data from advance detectors is available. Therefore, in this case, we can only have rough estimates of traffic states for through and right-turn movements. Furthermore, loop detectors are not always in good health. Even with complete detector coverage, poor data quality also reduces the reliability of the estimated traffic states. Therefore, in the near future, we are interested in bringing more data types, e.g., probe trajectories, and fusing them with loop detectors to have more robust and accurate estimates of traffic states.

References

[1] Al-Ghamdi, A., 1999. Entering headway for through movements at urban signalized intersections. *Transportation Research Record: Journal of the Transportation Research Board (1678), 42–47*.

[2] Bando, M., Hasebe, K., Nakanishi, K., Nakayama, A., Shibata, A., Sugiyama, Y., 1995. Phenomenological study of dynamical model of traffic flow. *Journal de Physique I 5 (11), 1389-1399.*

[3] Transportation Research Board, 2000. Highway Capacity Manual. *National Research Council, Washington, DC.*

[4] Buisson, C., Ladier, C., 2009. Exploring the impact of homogeneity of traffic measurements on the existence of macroscopic fundamental diagrams. *Transportation Research Record: Journal of the Transportation Research Board 2124, 127–136.*

[5] Cassidy, M. J., 1998. Bivariate relations in nearly stationary highway traffic. *Transportation Research Part B: Methodological 32 (1), 49–59.*

[6] Castillo, J. D., Benitez, F., 1995. On the functional form of the speed-density relationship II: empirical investigation. *Transportation Research Part B: Methodological 29 (5), 391–406.*

[7] Cheung, S. Y., Coleri, S., Dundar, B., Ganesh, S., Tan, C.-W., Varaiya, P., 2005. Traffic measurement and vehicle classification with single magnetic sensor. *Transportation Research Record 1917 (1), 173–181.*

[8] Daganzo, C. F., Gayah, V. V., Gonzales, E. J., 2011. Macroscopic relations of urban traffic variables: Bifurcations, multivaluedness and instability. *Transportation Research Part B 45 (1), 278–288.*

[9] Daganzo, C. F., Geroliminis, N., 2008. An analytical approximation for the macroscopic fundamental diagram of urban traffic. *Transportation Research Part B 42 (9), 771–781.*

[10] Dervisoglu, G., Gomes, G., Kwon, J., Horowitz, R., Varaiya, P., 2009. Automatic calibration of the fundamental diagram and empirical observations on capacity. *In: Transportation Research Board 88th Annual Meeting. No. 09-3159.*

[11] Edie, L. C., 1961. Car-following and steady-state theory for non-congested traffic. *Operations Research 9 (1), 66–76.*

[12] Gan, Q.-J., 2014. Macroscopic modeling and analysis of urban vehicular traffic (Chapter 6). *University of California, Irvine.*

[13] Gan, Q., Gomes, G. and Bayen, A., 2017. Estimation of Performance Metrics at Signalized Intersections Using Loop Detector Data and Probe Travel Times. *IEEE Transactions on Intelligent Transportation Systems, 18(11), pp.2939-2949.*

[14] Gan, Q.J., Jin, W.L. and Gayah, V.V., 2017. Analysis of traffic statics and dynamics in signalized networks: a poincaré map approach. *Transportation Science, 51(3), pp.1009-1029*.

[15] Gayah, V., Daganzo, C., 2011a. Effects of turningmaneuvers and route choice on a simple network. *Transportation Research Record: Journal of the Transportation Research Board 2249, 15–19.*

[16] Gayah, V. V., Daganzo, C. F., 2011b. Clockwise hysteresis loops in the macroscopic fundamental diagram: An effect of network instability. *Transportation Research Part B 45 (4), 643–655.*

[17] Geroliminis, N., Daganzo, C. F., 2008. Existence of urban-scale macroscopic fundamental diagrams: Some experimental findings. *Transportation Research Part B 42 (9), 759–770.*

[18] Geroliminis, N., Sun, J., 2011. Properties of a well-defined macroscopic fundamental diagram for urban traffic. *Transportation Research Part B 45 (3), 605–617.*

[19] Greenberg, H., 1959. An analysis of traffic flow. *Operations research 7 (1), 79–85.*

[20] Greenshields, B. D., Bibbins, J., Channing, W., Miller, H., 1935. A study of traffic capacity. *In Highway research board proceedings.*

[21] Helbing, D., 2009. Derivation of a fundamental diagram for urban traffic flow. *The European Physical Journal B 70 (2), 229–241.*

[22] Herman, R. and Prigogine, I., 1979. A two-fluid approach to town traffic. *Science, 204(4389), pp.148-151.*

[23] Ji, Y., Daamen, W., Hoogendoorn, S., Hoogendoorn-Lanser, S., Qian, X., 2010. Investigating the shape of the macroscopic fundamental diagram using simulation data. *Transportation Research Record: Journal of the Transportation Research Board 2161, 40–48.*

[24] Jin, W.-L., Gan, Q.-J., Gayah, V. V., 2013. A kinematic wave approach to traffic statics and dynamics in a double-ring network. *Transportation Research Part B 57, 114–131.*

[25] Jin, X., Zhang, Y., Wang, F., Li, L., Yao, D., Su, Y., Wei, Z., 2009. Departure headways at signalized intersections: A log-normal distribution model approach. *Transportation research part C: emerging technologies 17 (3), 318–327.*

[26] Knoop, V., Hoogendoorn, S., Van Lint, J. W., 2012. Routing strategies based on macroscopic fundamental diagram. *Transportation Research Record: Journal of the Transportation Research Board 2315, 1–10.*

[27] Li, J., Zhang, H. M., 2011. Fundamental diagram of traffic flow. *Transportation Research Record: Journal of the Transportation Research Board 2260 (-1), 50–59.*

[28] Lin, F.-B., Thomas, D., 2005. Headway compression during queue discharge at signalized intersections. *Transportation Research Record: Journal of the Transportation Research Board (1920), 81–85.*

[29] Liu, H.X., Wu, X., Ma, W. and Hu, H., 2009. Real-time queue length estimation for congested signalized intersections. Transportation research part C: emerging technologies, 17(4), pp.412-427.

[30] Lu, X.-Y., Varaiya, P., Horowitz, R., 2009. Fundamental diagram modeling and analysis based on ngsim data. *In: 12th IFAC Symposium on Control in Transportation System. pp. 2–4.*

[31] Mazloumian, A., Geroliminis, N., Helbing, D., Mazloumian, A., Geroliminis, N., Helbing, D., 2010. The spatial variability of vehicle densities as determinant of urban network capacity. *Philosophical Transactions of the Royal Society A: Mathematical, Physical and Engineering Sciences 368 (1928), 4627–4647.*

[32] Newell, G., 2002. A simplified car-following theory: a lower order model. *Transportation Research Part B: Methodological 36 (3), 195–205.*

[33] Newell, G. F., 1961. Nonlinear effects in the dynamics of car following. *Operations Research 9 (2), 209–229.*

[34] Payne, H.J., 1977. Discontinuity in equilibrium freeway traffic flow. *Transportation Research Record.*

[35] Pipes, L., 1953. An operational analysis of traffic dynamics. *Journal of applied physics 24 (3), 274–281.*

[36] Pipes, L., 1967. Car following models and the fundamental diagram of road traffic. *Transportation Research 1 (1), 21–29.*

[37] Skabardonis, A. and Geroliminis, N., 2008. Real-time monitoring and control on signalized arterials. Journal of Intelligent Transportation Systems, 12(2), pp.64-74.

[38] Tong, H., Hung, W., 2002. Neural network modeling of vehicle discharge headway at signalized intersection: model descriptions and results. *Transportation Research Part A: Policy and Practice 36 (1), 17–40.*

[39] Wu, X., Liu, H. X., Geroliminis, N., 2011. An empirical analysis on the arterial fundamental diagram. *Transportation Research Part B: Methodological 45 (1), 255–266.*

[40] Yan, Q., Sun, Z., Gan, Q., Jin,W.-L., 2018. Automatic identification of near-stationary traffic states based on the pelt changepoint detection. *Transportation Research Part B: Methodological 108, 39–54.*